Sensitivity of Ozone Production to NO_x and VOC along the Lake Michigan Coastline

Michael P. Vermeuel[1], Gordon A. Novak[1], Hariprasad D. Alwe[2], Dagen D. Hughes[3], Rob Kaleel[4], Angela F. Dickens[5], Donna Kenski[4], Alan Czarnetzki[6], Elizabeth A. Stone[3], Charles O. Stanier[7], R. Bradley Pierce[8,] Dylan B. Millet[2], Timothy H. Bertram[1,*]

[1]Department of Chemistry, University of Wisconsin, Madison, WI, USA;
[2]Department of Soil, Water, and Climate, University of Minnesota, St. Paul, MN, USA;
[3]Department of Chemistry, University of Iowa, Iowa City, IA, USA;
[4]Lake Michigan Air Directors Consortium, Rosemont, IL, USA;
[5]Wisconsin Department of Natural Resources, Madison, WI, USA;
[6]Department of Earth and Environmental Sciences, University of Northern Iowa, Cedar Falls, IA, USA;
[7]Department of Chemical and Biochemical Engineering, University of Iowa, Iowa City, IA, USA;
[8]Space Science and Engineering Center, University of Wisconsin, Madison, WI, USA;
*Correspondence to: T.H. Bertram, timothy.bertram@wisc.edu

Key Points

- Direct observations of H_2O_2/HNO_3 at an urban plume endpoint can be used to assess the integrated O_3 sensitivity to NO_x and VOC emissions.
- Indicators of O_3 sensitivity show that the urban plume traveling over Lake Michigan evolves from VOC towards NO_x sensitive O_3 production.
- O_3, H_2O_2, HNO_3, and NO_3^- provide unique constraints to predict the response of O_3 to changes in VOC and NO_x emissions in coastal regions.

Abstract

We report on the sensitivity of enhanced ozone (O_3) production, observed during lake breeze circulation along the coastline of Lake Michigan, to the concentrations of nitrogen oxides (NO_x = NO + NO_2) and volatile organic compounds (VOCs). We assess the sensitivity of O_3 production to NO_x and VOC on a high O_3 day during the Lake Michigan Ozone Study 2017 (LMOS 2017) using an observationally-constrained chemical box model that implements the Master Chemical Mechanism (MCM v3.3.1) and recent emission inventories for NO_x and VOCs. The MCM model is coupled to a backward air mass trajectory analysis from a ground supersite in Zion, IL where an extensive series of measurements of O_3 precursors and their oxidation products, including hydrogen peroxide (H_2O_2), nitric acid (HNO_3), and particulate nitrates (NO_3^-) serve as model constraints. We evaluate the chemical evolution of the Chicago-Gary urban plume as it advects over Lake Michigan and demonstrate how modeled indicators of VOC- *vs.* NO_x- sensitive regimes can be constrained by measurements at the trajectory endpoint. Using the modeled ratio of the instantaneous H_2O_2 and HNO_3 production rates (P_{H2O2} / P_{HNO3}), we suggest that O_3 production over the urban source region is strongly VOC-sensitive and progresses towards a more NO_x-sensitive regime as the plume advects north along the Lake Michigan coastline on this day. We also demonstrate that ground-based measurements of the mean concentration ratio of H_2O_2 to HNO_3 describe the sensitivity of O_3 production to VOC and NO_x as the integral of chemical production along the plume path.

1. Background

Regulating the concentration of surface ozone (O_3) is necessary to maintain and improve public health and agriculture. At elevated concentrations, long-term exposure to O_3 is linked to increased mortality in humans from respiratory illnesses (Jerret et al., 2009) and the slowing of stomatal responses in plants to harsh environmental conditions (Mills et al., 2009). Short-term exposure to O_3 results in the inflammation of bronchial airways and acute lung damage (Devlin et al., 1991; Gauderman, 2006). To prevent these adverse effects, the U.S. Environmental Protection Agency (EPA) enforces National Ambient Air Quality Standards (NAAQS) for O_3 and particulate matter. A monitoring site is deemed compliant with the O_3 NAAQS if its maximum daily 8-hr average (MDA8) is at or below 70 ppbv ; a standard that has proven difficult to achieve for certain parts of the United States (US EPA, 2015). Effective regulation of O_3 concentrations is challenging due to

the complex nonlinear chemistry involved in ozone production. This complex chemistry makes it difficult to predict the response of O_3 to changing emissions of its precursors, NO_x and VOCs (Travis et al., 2016).

Key to predicting high pollution events is the ability to determine how the production rate of O_3 (P_{O3}), which is driven by regional chemical sources (e.g. industrial point sources, on-road emissions, large urban sectors), is enhanced by local meteorological processes. The links between these factors are particularly important in coastal areas. Depending on local winds, emissions can be advected offshore, chemically processed in the shallow, stable boundary layer over a body of water and then advected onshore to produce high pollution events due to lake breeze circulation (Foley et al., 2011). Coastal regions in the U.S. where this phenomenon has been observed include Lake Michigan (Dye et al., 1995), Lake Erie (Brook et al., 2013), the Gulf of Mexico (Mazzuca et al., 2016), and the Chesapeake Bay (Loughner et al., 2014; Stauffer & Thompson, 2012; Sullivan et al., 2019). There is still significant uncertainty regarding the conditions driving coastal O_3 production, which limits confidence in proposed emission control strategies for reducing O_3 exceedances in such regions. In this study, we explore the use of indicator ratios based on ambient observations for describing the sensitivity of O_3 production to VOC and NO_x emissions in coastal regions along Lake Michigan.

Here, we briefly review the photochemistry of tropospheric O_3 formation that serves as the chemical basis for the utility of indicator ratios. Section 1 (S1) of the Supporting Information (SI) gives a detailed review of this photochemistry along with derivations of key equations. The photochemical production of O_3 is regulated by the concentrations of NO_x and hydrogen oxide radicals (HO_x = OH + HO_2) and relies on the catalytic cycling of NO_x between NO and NO_2 and of HO_x between the hydroxyl radical (OH), the hydroperoxyl radical (HO_2) and organic peroxy radicals (RO_2) (Jacob, 1999).

Chain termination of the O_3 cycle depends on the relative abundances of HO_x and NO_x. At the limit of high HO_x and low NO_x, the major chain terminating reactions are:

$$HO_2 + HO_2 + M \rightarrow H_2O_2 + O_2 + M \quad (R1)$$

$$HO_2 + RO_2 \rightarrow ROOH + O_2 \quad (R2)$$

where H_2O_2 and ROOH are hydrogen peroxide and hydroperoxides, respectively, and M is any non-reactive species that stabilizes the product through collisions. In this chemical regime, the steady state concentration of HO_x is insensitive to changing NO_x and O_3 production increases linearly with NO_x. Because of this, when R1 and R2 dominate chain termination, O_3 production is said to be NO_x-sensitive. In contrast, when peroxy radical (HO_2 + RO_2) removal is dominated by reactions with NO_x, chain termination results in formation of HNO_3, alkyl nitrates ($RONO_2$), peroxynitrates (RO_2NO_2), and peroxy acylnitrates (RCO_3NO_2):

$$OH + NO_2 + M \rightarrow HNO_3 + M \quad (R3)$$

$$RO_2 + NO + M \rightarrow RONO_2 + M \quad (R4)$$

$$RO_2 + NO_2 + M \rightarrow RO_2NO_2 + M \quad (R5)$$

$$RCO_3 + NO_2 + M \rightarrow RCO_3NO_2 + M \quad (R6)$$

where RCO_3 is a peroxyacyl radical. If the HO_x-NO_x cycle is primarily terminated through R3-R6, O_3 production is VOC-sensitive. In this regime, the rate of O_3 formation increases with increasing VOC and is suppressed by increasing NO_x (Milford et al., 1989).

Due to their status as chain termination products for these two limiting regimes, H_2O_2 and HNO_3 can be employed as indicator species. It should be noted that in regions of high biogenic emissions contributions from R2 and R4 are important. Specifically, the quantities H_2O_2/HNO_3 (concentration ratio) and P_{H2O2}/P_{HNO3} (production ratio) can serve as time-integrated or instantaneous indicators of the sensitivity of O_3 production to VOC or NO_x emissions (Sillman, 1995) (Tonnesen & Dennis, 2000). Sillman et al. (1990) first showed the utility of such indicators by modeling the sources and sinks of odd hydrogen along with the corresponding O_3 production. A linkage between P_{H2O2}, P_{HNO3}, and NO_x *vs* VOC limited O_3 production, as defined by the coupled HO_x-NO_x reactions, can be established by assuming that HO_x is in steady-state and HO_x production equals HO_x loss ($P_{HOx} = L_{HOx}$) (Lurmann et al., 1986; Sillman et al., 1990).

To arrive at a robust indicator value utilizing these termination species, photochemical simulations with varying rates of anthropogenic and biogenic emissions as well as changing meteorological conditions have been previously performed for several test scenarios. Models of O_3-NO_x-VOC sensitivity utilizing the indicator ratios of H_2O_2/HNO_3 and P_{H2O2}/P_{HNO3} have shown that the transition from VOC-sensitive to NO_x-sensitive O_3 production occurs in the regime where the

concentration ratio value is between 0.06-0.35 at peak O_3 concentrations (Sillman & West, 2009; Sillman, 2002; Tonnesen & Dennis, 2000). However, there is still a need to explore how these values map to traditional definitions of NO_x- and VOC- sensitive O_3 production in more complex environments. An advantage of the H_2O_2/HNO_3 indicator is that it can be directly measured, serving as a unique observation-based constraint. Ground-based measurements of daytime (9:00-17:00) [H_2O_2] and [HNO_3] have been used previously to identify stationary O_3 sensitivity regimes in southern Taiwan where the reported averaged rural and urban spring [H_2O_2] was 2.6 and 1.0 ppbvv respectively and the reported averaged rural and urban springtime [HNO_3] reported to be 3.0 and 5.1 ppbvv respectively (Peng et al., 2006, 2011). Alternatively, the ratio of production rates (P_{H2O2}/P_{HNO3}) could be used as a measure of the sensitivity of P_{O3} to changing NO_x and VOC emissions in spatially and temporally evolving air masses as it is the ratio of two instantaneous production rates. In urban areas or areas of low BVOC (biogenic volatile organic compounds), this ratio can be approximated as:

$$\frac{P(H_2O_2)}{P(HNO_3)} = \frac{k_4[HO_2]^2}{k_6[OH][NO_2]} \quad (E1)$$

From E1 it is clear that: 1) direct constraints on the production rates require measurements of NO_x and HO_x species and 2) the indicator serves as an instantaneous measure of the sensitivity of P_{O3} to NO_x and VOC concentrations.

The indicator L_N/Q is analogous to P_{H2O2}/P_{HNO3} and focuses on radical production rates (Q) and the fraction of radicals removed by reactions with NO_x (L_N). When L_N is estimated as the combined rates of R3 + R4 and Q from the combined rates of radical initiation stemming from O_3 and carbonyl photolysis (Kleinman, 2005), the ratio L_N/Q can be calculated as:

$$\frac{L_N}{Q} = \frac{k_6[OH][NO_2] + k_7[RO_2][NO]}{A[O_3] + B[RH]} \quad (E2)$$

where A and B are effective rate coefficients that account for sources of HO_x from photolysis of O_3 and carbonyls respectively, C is an effective rate coefficient that accounts for formaldehyde and carbonyl formation (Lurmann et al., 1986; Sillman et al., 1990). It has been proposed that when L_N/Q is less than 0.5, P_{O3} is NO_x-sensitive and when L_N/Q is greater than 0.5, P_{O3} is VOC-sensitive (Kleinman et al., 2001). The transition region or cutoff value for VOC-NO_x sensitivity depends on the contribution of organic nitrates to L_N, thus allowing the cutoff value of 0.5 to vary

depending on the environment (Kleinman, 2005). Calculations of L_N/Q are ideal for an urban plume as they convey information on the sensitivity regime of an air parcel that generally transitions from high NO_x at the source to low NO_x some distance away. Relating P_{O3} and the sensitivity regime using this indicator requires both constrained quantities of measured chemical species in HO_x-NO_x cycling as well as confident predictions of meteorology and chemical unknowns. For that reason, L_N/Q is underutilized and not included in many field-based analyses (Kleinman et al., 2000; Mazzuca et al., 2016).

In this study, we explore the use of indicator ratios based on the concentration and production rates of H_2O_2 and HNO_3 for describing the sensitivity of O_3 production to VOC and NO_x emissions during O_3 exceedance episodes in coastal regions along Lake Michigan. NO_x and VOC emissions along the Lake Michigan shoreline are both spatially and temporally heterogeneous due to both urban (S2; Fig S1) and rural sources and the extent to which changing biogenic and anthropogenic emissions influence P_{O3} is still unclear. To address these issues, we conducted the Lake Michigan Ozone Study (LMOS) in late spring 2017 (Pierce et al., 2017). This late spring measurement period was chosen as it is historically the time of year when the Lake Michigan region experiences peak ozone concentrations. This project was a collaborative, multi-agency field study that utilized ground-based, airborne, and remote sensing measurements in various parts of the Lake Michigan shoreline. The LMOS 2017 study was conducted 26 years after the first Lake Michigan ozone study (Dye et al., 1995) and the multi-platform measurements conducted during LMOS 2017 provide an opportunity to interrogate the region's current ozone chemistry that results in high ozone events despite decades of steady decreases in ozone precursor emissions. A field site in Zion, IL, located along the shoreline near the Illinois/Wisconsin border, served as a ground site for continuous monitoring of both O_3 precursors and termination products, including the cycle termination products H_2O_2 and HNO_3. In this analysis, we utilize the continuous measurements at the Zion site as constraints for trajectory-based chemical box models to define the spatial and temporal evolution of O_3-VOC-NO_x sensitivity of an urban plume of high observed O_3 and NO_x undergoing lake breeze circulation. These measurements also provide an opportunity to contrast time-integrated concentration ratios and instantaneous chemical rates as indicators of O_3-VOC-NO_x sensitivity for future studies.

2. Methods

2.1 The Zion Supersite

The Zion ground site was located in Illinois Beach State Park, Zion, IL, (42.47 °N, 87.81 °W), 890 m to the west of the Lake Michigan shoreline and 60 km north of Chicago. The terrain of the park consists of marshes, dunes, grassland prairies, and forests of black oak amongst mixed vegetation. Measurements at this site were conducted from 22 May to 22 June 2017. Two trailers, one of which is a continuous O_3 ground monitor site, were provided by Illinois EPA (IEPA) for housing of the instrumentation. The Lake Michigan Air Directors Consortium (LADCO) maintained a suite of equipment for meteorological measurements: wind speed and direction, solar radiation, rainfall, temperature, and dew point. Additional gas-phase measurements during the intensive sampling period included: NO and NO_2 (Chemiluminescence, Thermo Fisher 42i); non-methane VOCs measured both *in situ* by Proton Transfer Reaction Quadrupole Interface Time-of-Flight Mass Spectrometer (PTR-QiToF, Ionicon Analytik) as described by Millet et al. (2018) and offline by GC-MS following canister collection every four hours during predicted high ozone events (Schauffler et al., 1999); termination products of HO_2, RO_2, and NO_x (e.g., H_2O_2 and HNO_3) measured using chemical ionization mass spectrometry that is discussed in more detail in the following paragraph and in the SI (S3-S4). At the measurement site, local influences impact the uncertainty of H_2O_2 and are explained in 3.1. *In situ* measurements of aerosol particle size distributions and offline measurements of particle chemical composition were made during the intensive sampling period. Aerosol particles less than 2.5 microns were collected on filter substrates for subsequent quantification of particle mass, elemental and organic carbon (EC and OC), organic species, and water soluble metals, anions and cations in polluted and non-polluted air masses (Stone et al., 2008). Aerosol optical depth products were retrieved using an Aeronet sun photometer deployed at Zion from 4-22 June 2017. Particle phase nitrate was measured by ion chromatography following aqueous extraction (Jayarathne et al., 2014). Water vapor and temperature profiles up to 10 km above ground were retrieved with a microwave radiometer and wind profiles from 30 m to 200 m above ground were made using SODAR.

Mixing ratios of H_2O_2 and HNO_3 were measured by Chemical Ionization Time-of-Fight Mass Spectrometry (CI-ToFMS, Tofwerk AG, Switzerland, and Aerodyne Research Inc., USA) alternating between O_2^- and I^- reagent ion chemistry for the detection of H_2O_2 and HNO_3,

respectively. Product ions are generated at high pressures (75-90 mbar) and transmitted through multiple stages of differential pumping prior to orthogonal extraction into a compact time of flight mass analyzer (ToFMS). A more complete description of the instrument and its operation is provided by Bertram et al. (2011). HNO_3 was detected as the cluster $[I \cdot HNO_3]^-$ at m/Q 190 and H_2O_2 was detected as $[O_2 \cdot H_2O_2]^-$ at m/Q 66. More details on field operations as well as sensitivities for both product ions and their dependence on specific humidity (SH) are included in the SI sections S3-S4 (Fig S2-S7).

2.2 Trajectory Model

A trajectory box model was built in MATLAB that incorporates the Framework for 0-D Atmospheric Modeling (F0AM) (Wolfe et al., 2016) to calculate mixing ratios and reaction rates of important compounds involved in O_3 production along air parcel trajectories. The model operates over a domain spanning 41 to 45°N latitude and 89 to 85°W longitude, and is driven by analyzed winds with a model spatial resolution of 4 km and a temporal resolution of 1 hour. The volume of each photochemical box is set by the domain spatial resolution and from boundary layer depth outputs of the National Oceanic and Atmospheric Administration (NOAA) High-Resolution Rapid Refresh (HRRR) model (Smith et al., 2008). The chemistry used in each box is from the Master Chemical Mechanism (MCM v3.3.1) that can simulate up to 17,224 reactions amongst 5,832 chemical species with integrated photolysis rates (Saunders et al., 2003). In this applied model 2,756 species and 8,401 reactions were used to optimize performance while still covering the predominant species in urban chemistry.

To simulate the chemistry in an urban plume evolving along a trajectory towards Zion, IL, regional anthropogenic and biogenic emissions were incorporated along with observed meteorological parameters. Anthropogenic stationary and non-stationary emissions of hourly weekday speciated NO_x and VOC were gathered from the EPA National Emissions Inventory (NEI) 2014 at 12 km resolution. VOC emissions are speciated into 21 compounds of different functional groups and bond order. Biogenic emissions were calculated using a combination of model and ground-based constraints for equations estimating the net emission rate of isoprene in the Model of Emissions of Gases and Aerosols from Nature (MEGAN) found in Guenther, et al. (2006). Select ground-based

measurements of NO_x and VOC from the EPA Photochemical Assessment Monitoring Stations (PAMS) network also provided chemical constraints to be discussed in section 3.3.

The meteorological factors required for estimating biogenic emissions as well as calculating chemical and photolytic rates were gathered for each grid in the model as follows. Temperature, surface wind, and relative humidity fields were generated by interpolating hourly meteorological ground-based field measurements from the EPA Airnow Remote Sensing Information Gateway (RSIG) and the EPA Air Quality System (AQS). Over the lake, temperature, pressure, and relative humidity are estimated from low-level aircraft flights. Lake Michigan surface water temperatures were taken from the NOAA Great Lakes Surface Environmental Analysis (GLSEA) and interpolated from the 6-hourly product to an hourly resolution on a 1.3 km grid. More details on model constraints are found in SI section S5 (Fig. S8).

Air parcel trajectories were determined from the NOAA Hybrid Single-Particle Lagrangian Integrated Trajectory (HYSPLIT) model running HRRR (Stein et al., 2015). An air parcel path is generated by retrieving a backward trajectory from the NOAA Real-time Environmental Display sYstem (READY) (Rolph et al., 2017) with a start point at the surface (20 m) in Zion, IL and an end point 10 hours prior to the start. The chemical model is evaluated starting at the backward trajectory endpoint and moving forward toward the Zion site. An example trajectory for 2 June 2017 ending at Zion, IL at 17:00 CDT is displayed in Figure S13 along with observed and modeled constraints within the domain on 2 June at 12:00 CDT. Chemistry is solved along the trajectory by treating the first grid on the trajectory as a stationary point. Modeled constraints up to 24 hours prior are used to allow this box to spin up for six days to reach steady state concentrations of chemical intermediates. Once the first box is at steady state, the resulting outputs are used as initial conditions for the next step in the trajectory. Box models are solved hourly along each point on the trajectory and the integrated mixing ratios of the entire trajectory are compared to the Zion field measurements.

3. Results

3.1 H_2O_2 and HNO_3 Measurements at Zion, IL

The time series of H_2O_2, isoprene, HNO_3, O_3 and NO_x mixing ratios along with ambient temperature and solar radiation at Zion, IL, for the month of June are shown in Figure 1. The time series of isoprene mixing ratios indicates that the influence of BVOC emissions on the Zion sampling site is periodic, where BVOC emissions peak with photosynthetically active radiation and the daytime maximum mixing ratio increases with warmer temperatures in the later parts of the month. The relative increase in the mixing ratios of H_2O_2 and isoprene are coherent in time, reflecting the role of H_2O_2 as a termination product of HO_x cycling in BVOC rich air. Mixing ratios of isoprene range from 0.3-6.6 ppbv during the daytime with a mean daily maximum of 1.2 ppbv (Fig. S9). Daytime mixing ratios of H_2O_2 and HNO_3 ranged from 0.5-8 ppbv and 0.1-6 ppbv, with average midday mixing ratios of 2.1 ppbv and 1.1 ppbv, respectively (Fig S10).

A strong diel profile in HNO_3 and H_2O_2 mixing ratios is observed at Zion, due to a combination of photochemical sources and short atmospheric lifetimes at the surface (Fig. S10). The shape of the HNO_3 diel profile diverges slightly from that expected for local photochemical production, due to complex meteorological patterns in the coastal region and the arrival of the Chicago-Gary urban plume during periods of lake breeze circulation. In the time period from 6-18 June 2017, when ambient temperatures and biogenic emissions increase, sustained mixing ratios of H_2O_2 are observed at night ($[H_2O_2]_{night,mean}$ = 2.0 ppbv). Elevated nocturnal H_2O_2 mixing ratios may indicate that: 1) a molecule that is isobaric with the $O_2^{-}{\cdot}H_2O_2$ ion (66 m/Q) is present at high abundance, resulting in an overestimate of H_2O_2 or 2) ozonolysis of biogenic alkenes sustains local nocturnal H_2O_2 production resulting in elevated H_2O_2 mixing ratios at night while deposition is also suppressed. While the source of the nocturnal H_2O_2 signal is unknown at this time, we do not expect it to significantly impact the analysis that follows as we focus largely on observations during the daytime ($J_{NO2} > 5 \times 10^{-5}$ s^{-1}) and on detailed trajectory analyses for periods before 7 June, when nocturnal H_2O_2 concentrations were small.

The mixing ratio of O_3 at Zion follows a strong diel profile (Fig. S11), peaking in the early evening and regularly exceeding 60 ppbv throughout the measurement period. Daily maximum 8-hour average concentrations exceeded the NAAQS level of 70 ppbv on 2 and 15 June at 79 and 73 ppbv, respectively. The largest O_3 episode occurred on 2 June which correlated with an increase in NO_x. NO_x mixing ratios do not show a consistent diel profile (Fig S11), but display large day-to-day differences, pointing to a combination of local sources and a regional background. Influences of

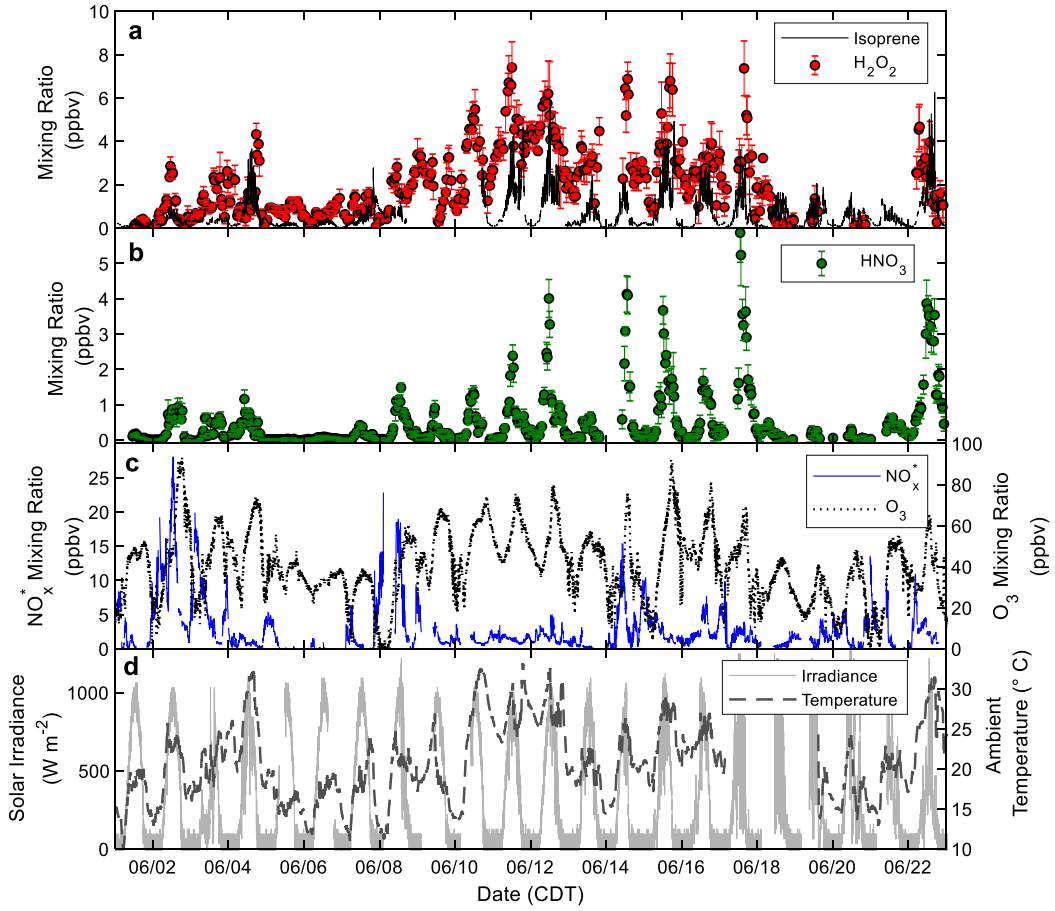

Figure 1: Time series of chemical measurements at Zion, IL taken between 1-23 June 2017. a) Isoprene and H_2O_2 mixing ratios are broadly correlated with higher ambient temperatures, most notably following 10 June. b) HNO_3 mixing ratios follow a clear diel pattern, peaking in the late afternoon. c) The observed time series in NO_x^* mixing ratios revealed inconsistent diel patterns suggesting contribution from a wide number of local and regional sources. O_3 mixing ratios followed a classic diel profile with regular exceedances of 60 ppbv. d) Measurements of temperature and solar irradiance. H_2O_2 and HNO_3 is presented as 30-minute averages with an uncertainty of 1σ. All other data is presented with 1-minute resolution.

307 NO_x in this region can be both continental (e.g. vehicular and point source emissions) and marine
308 (e.g. recreational craft, ferries, cargo ships).
309
310 The reported NO_2 is not a true NO_2 measurement and likely contains a larger fraction of NO_y that
311 is converted to NO on the molybdenum oxide (MoO) catalytic converter (Fehsenfeld et al., 1987;
312 Williams et al., 1998; Xu et al., 2013) prior to detection *via* chemiluminescence. The positive
313 interferences for NO_2 and NO_x caused by this partial conversion of NO_z require us to refer to the
314 measured NO_2 and NO_x hereafter as NO_2^* and NO_x^*, as they are not true NO_x measurements for
315 the entire measurement period. Uncertainties in NO_x mixing ratios, stemming from the partial
316 conversion of NO_z ($NO_z = NO_y - NO$) are addressed through comparison of the
317 chemiluminescence NO_x measurement to the CI-ToFMS NO_2 signal using O_2^- chemistry (S4.2;
318 Fig. S12). It was determined that for the 2 June 17:00 CDT case study, the CIMS and
319 chemiluminescence NO_2 measurements agree within 12%.
320
321 A first approximation of the sensitivity of ozone to VOC and NO_x, can be derived from the ratio
322 of H_2O_2 and HNO_3 mixing ratios between 9-19 CDT, during periods in June when the Zion site
323 received on-shore flow from Lake Michigan (wind directions between 45-165°, Fig. 2). This time
324 window was chosen based on typical timing of onshore lake breeze flow, as well as the period of
325 photochemical activity. However, the filter captures a mix of lake breeze driven onshore flow,
326 synoptically driven onshore flow, and air masses approaching from the south and south southwest
327 that may have not been processed over Lake Michigan. Based on the slope of each regression
328 ($m>1.5$) one might conclude that O_3 measured at Zion during these hours was produced in plumes
329 evolving under primarily NO_x-sensitive conditions as the slopes of H_2O_2/HNO_3 exceed the
330 threshold of 0.2 - 0.4 reported in Sillman et al. (1995; 1997). As we discuss in section 4, such an
331 interpretation is challenging for multiple reasons. Most importantly, the prescribed Sillman
332 indicator ratio ($H_2O_2/HNO_3 = 0.04$) was based on the ratio achieved at the hour of peak ozone
333 concentration, and addressed the sensitivity of ozone concentrations to perturbations in
334 anthropogenic NOx and VOC emissions. A primary objective of LMOS was to determine the
335 sensitivity of ozone to NO_x and VOC emissions during O_3 exceedance events, which are a small
336 subset of the data presented in Figure 2. To establish connections between ozone concentrations,

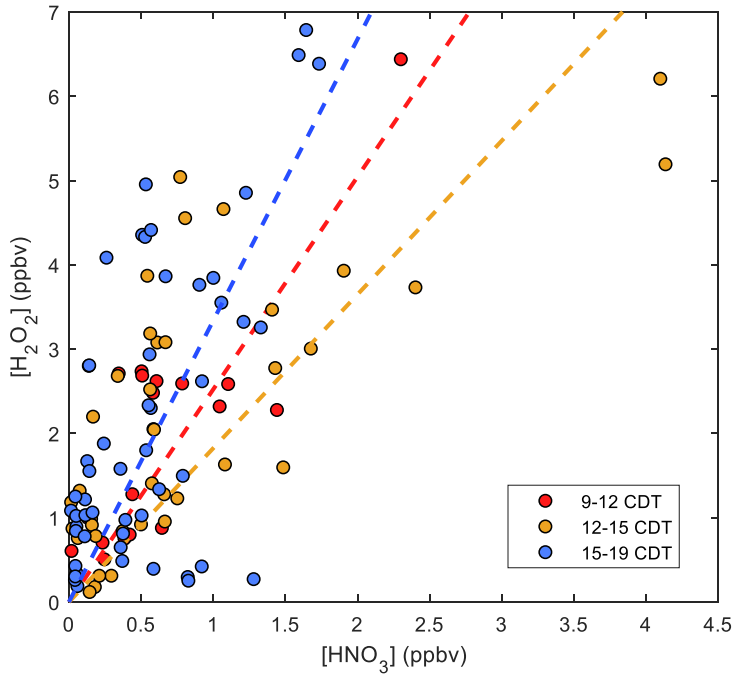

Figure 2: Regression of daytime (9:00-19:00 CDT) hourly-averaged H_2O_2 and HNO_3 mixing ratios during sustained periods (6 hours or more) of eastern and southeastern (45-165°) winds. The daytime was divided into three time periods (colored dots) and each were fit through the origin (dashed lines): 9-12 CDT (m= 2.5, R^2=0.64), 12-15 CDT (m=1.8, R^2=0.64), 15-19 CDT (m=3.3, R^2=0.55).

337 instantaneous P_{O3}, and the indicator ratios discussed above, we will focus on a case study of lake
338 breeze circulation where high O_3 and NO_x concentrations were observed (2 June 2017).
339
340
341 *3.2 Case Study: June 2nd Lake Breeze Event*
342 Figure 3 shows the time series of multiple concurrent measurements at Zion, IL during a lake
343 breeze event on Friday, 2 June 2017. This day was chosen for the model case study because: 1)
344 there was a sustained lake breeze for 10 hours, 2) measurements reported the highest O_3 and NO_x
345 at Zion for the length of the campaign, and 3) HNO_3 was sustained for the duration of the lake
346 breeze period, indicative of an aging urban plume being received onshore from an upwind polluted
347 region. Observations of wind speed and direction indicate that the mid-morning had offshore
348 northwesterly winds that were abruptly replaced by onshore southeasterly winds between 09:00
349 and 10:00 CDT. These onshore winds, accompanied by a sharp decrease in mixed layer height,
350 were maintained for 10 hours until dissipation around 20:00 CDT, indicative of a sustained deep

lake-land breeze. Measurements of NO_x^* indicate that NO_x-polluted urban air parcels were carried with the lake breeze, with mixing ratios peaking at 27.1 ppbv around 12:30 and then declining throughout the rest of the day. NOAA HYSPLIT HRRR backward trajectories starting at Zion, IL, confirm that this lake breeze period consists of multiple urban air parcels originating throughout the Gary, IN, and Chicago, IL, region (Fig. S13). Elevated HNO_3 concentrations were observed at

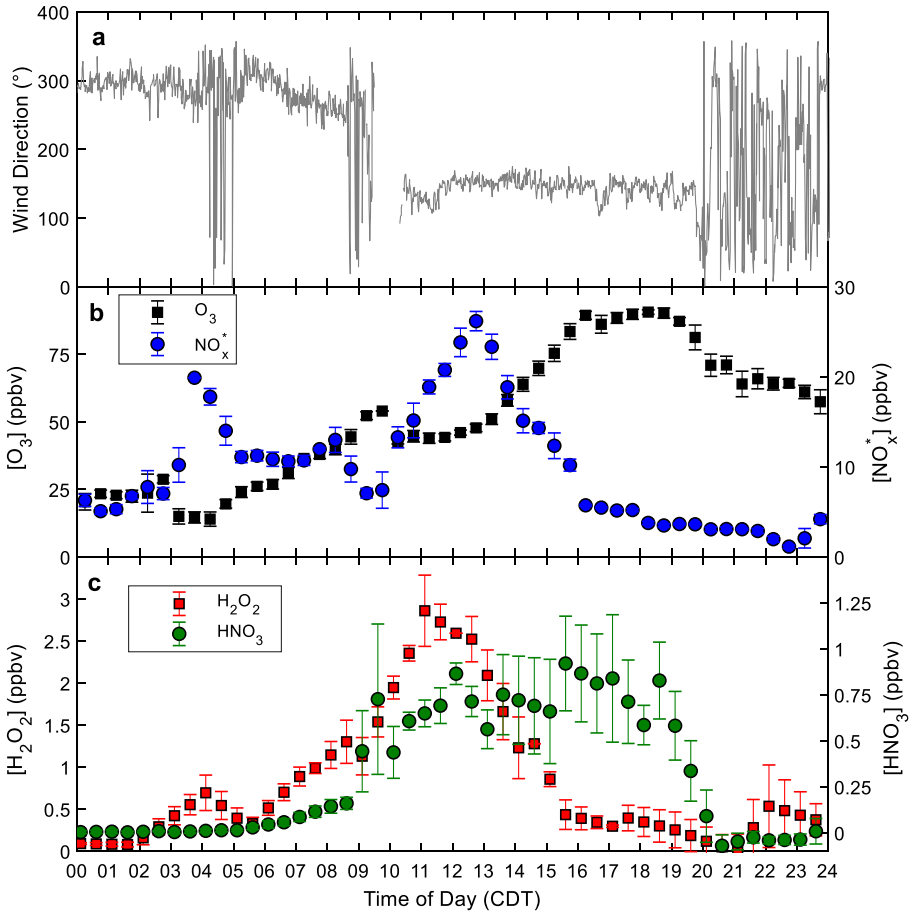

Figure 3: Time series of chemical measurements at Zion, IL during the lake breeze induced O_3 event on 2 June 2017. Blue shading indicates lake breeze period. a) Lake breeze commenced between 9:00 and 10:00 CDT as indicated by an abrupt switch from northwesterly winds to southeasterly winds. b) The resulting change in NO_x and O_3 are shown in blue and black, respectively. c) The mixing ratio of H_2O_2 (red) does not appear to respond significantly to the change in wind direction. HNO_3 (green) shows sustained mixing ratios until around 20:00 CDT when the lake breeze ends. Wind data is shown as 1-minute averages and chemical composition is shown as 30-minute averages with a variance of 1σ.

the onset of the lake breeze before declining abruptly at the end of the lake breeze event. H_2O_2

mixing ratios appeared to be largely independent of the change in wind direction following a classic diel profile.

The diel profile in O_3 on 2 June is characterized by two sequential periods of rapid increase in mixing ratio. The first period, occurring between 4:30–9:30 CDT, is characterized by a ΔO_3 of 41 ppbv (14 – 55 ppbv), or an averaged increase of 8.2 ppbv hr^{-1} prior to the onset of onshore winds at 09:30. Following the start of southwesterly winds, O_3 mixing ratios remain constant close to 48 ppbv until around 13:00 when there is a concurrent decline in NO_x. The second period of rapid increase in O_3 mixing ratio occurs between 13:00-16:00 CDT, peaking at 92 ppbv at 16:00, sustaining an average increase of 14.3 ppbv hr^{-1}. O_3 mixing ratios again remain nearly constant between 16:30-19:30 CDT before gradually decaying throughout the rest of the evening, with the largest drop in mixing ratio concurrent with the end of the lake breeze. Similar high O_3 events occurred on this day along the Lake Michigan shoreline, with 8-hour max O_3 values exceeding 70 ppbv from latitudes as far south as 41.7°N near Whiting, IL to as far north as 44.1°N near Manitowoc, WI (Fig. S14). In section 3.3 we describe the base case chemical box model used to analyze the evolving plume.

3.3 Base Case Chemical Box Model Outputs

The trajectory model used in this analysis (described section 2.3) focuses on the air parcel arriving at Zion at 17:00 during the second plateau in peak O_3. Based on the ΔO_3 observed at Zion between 13:00-17:00 CDT, it can be assumed that high production of O_3 occurs in this parcel allowing it to serve as a suitable test case for evaluating indicators of O_3-NO_x-VOC sensitivity in an urban plume under the influence of a lake breeze circulation. The parcel originates in the Tinley Park, IL region at 8:00 and passes through the Chicago metropolitan area, East Chicago, and Gary, IN; the latter two are both historically industrial hubs for steel and cement manufacturing facilities (Harrison & Winchester, 1971; Winchester & Nifong, 1971) and remain important emissions sources as documented in NEI 2014 point source data. In its 10-hour trajectory, the parcel spends the first 2 hours on land and then the next 7 hours over the lake until returning to land at Zion. Figure 4a and 4b show the modeled NO_x and O_3 mixing ratios calculated along the air parcel trajectory (colored circles). Time aligned ground-based measurements of O_3 from AQS are included and the locations are shown with black diamonds. The O_3 and NO_x^* as measured at Zion is also included. There is

388 good agreement between the few experimental and model values before entering the lake and after
389 exiting the lake. At 09:00 CDT the O_3 model output is 46 ppbv and the nearest monitor recorded
390 49 ppbv. Upon exit of the lake at 17:00 CDT, the model and Zion monitor O_3 mixing ratios were
391 91 and 89 ppbv respectively, and the model NO_x and measured NO_x^* mixing ratios at the Zion site
392 were 6.0 and 5.7 ppbv respectively. A second O_3 monitor at Kenosha, WI (13 km north of Zion)
393 recorded an O_3 mixing ratio of 93 ppbv at 17:00 CDT, showing little spatial variation between
394 sites.

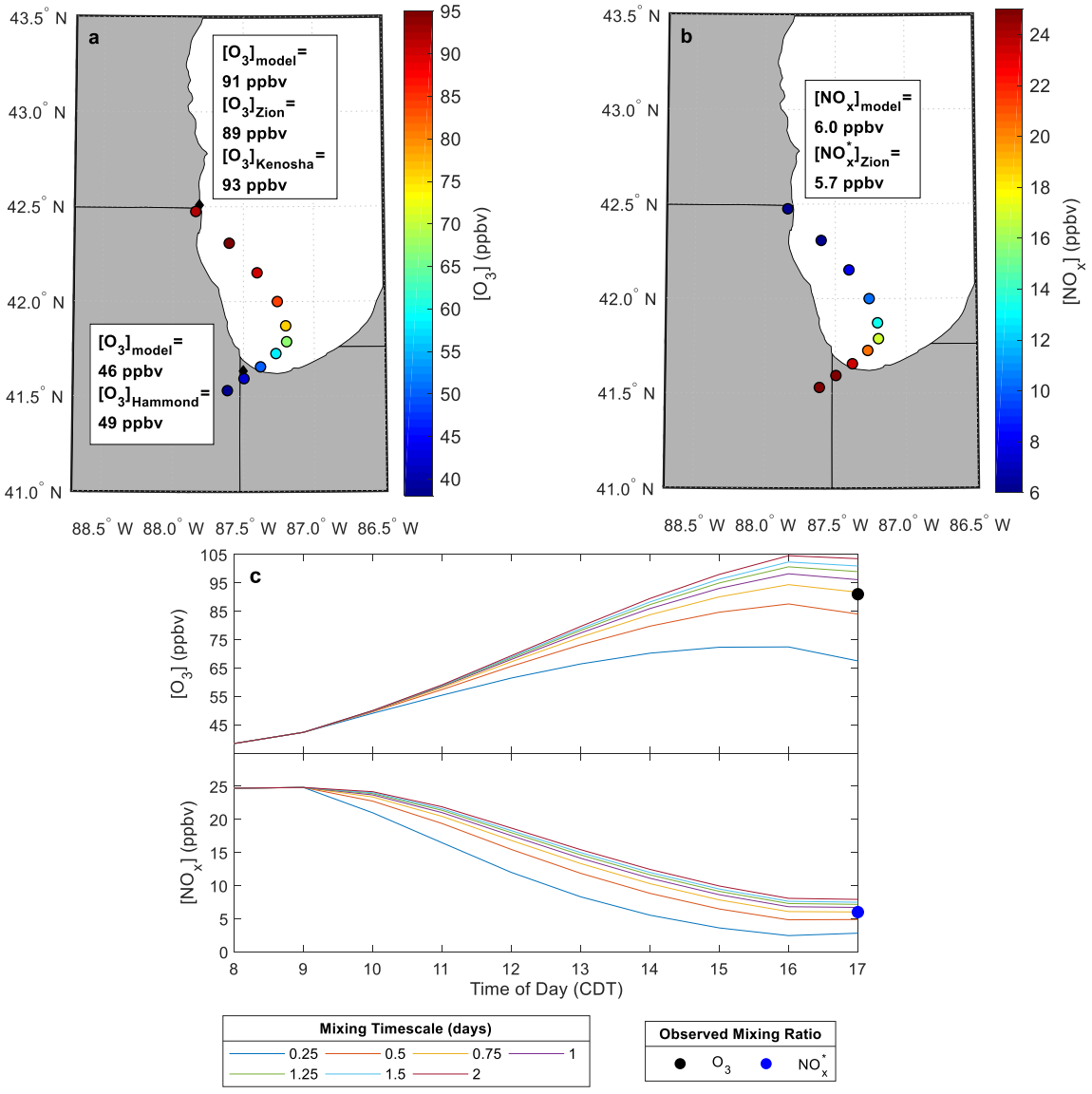

Figure 4: a,b) Trajectories of modeled O_3 and NO_x (colored circles) ending at the Zion site at 17:00 CDT. End point measurements of O_3 and NO_x* are shown with black diamonds. c) Sensitivity of modeled O_3 and NO_x mixing ratios to the prescribed mixing timescale τ_{mix} over the lake and onshore (10:00-17:00 CDT). Observations are consistent with a mixing timescale (τ_{mix}) of 0.75 days over the lake, considerably larger than that over land (ca. 0.20 days).

As discussed briefly in Section 2.2, the time evolution of each chemical in the box model is affected by both chemistry and mixing. In the MCM trajectory model, chemicals are subject to first order ventilation (Wolfe et al., 2016):

$$\frac{d[X]}{dt} = -k_{dil}([X] - [X]_b) \qquad (E3)$$

where k_{dil} is a first order dilution rate constant, [X] is the chemical concentration within the box, and $[X]_b$ is the background concentration. In the case of the evolving urban plume, k_{dil} is the rate of entrainment of background air and τ_{mix} (k_{dil}^{-1}) would be the e-folding time required to mix with the background. In the trajectory model, we determine $[X]_b$ over land from the average of background O_3 from AQS monitors and determine $[X]_b$ over the lake from the ensemble of aircraft and NOAA research vessel measurements near the surface of Lake Michigan. Daily land backgrounds of NO_x and VOC for the Chicago-Gary region were obtained from the EPA PAMS network. For the 2 June trajectories, the daily-averaged O_3, NO, and NO_2 land backgrounds as determined by AQS and the PAMS network were 42, 8.6, and 9.3 ppbv respectively. Background concentrations of O_3 in the model were the same over water as over land, but background NO_x and VOC over the lake were set to 0 ppbv. Low-level aircraft flights ($z<400$ m) on 2 June over Lake Michigan confirm that NO_x concentrations in background air are low ($[NO_2]_{mean}$=1.10 ppbv). Figure S16 shows the negligible impact of low background NO_x and VOC on $[O_3]$ during the case study trajectory. Limited horizontal mixing over the lake makes the contribution of background NO_x and VOC small. Unfortunately, there were no measurements of speciated VOCs in background air over the lake, thus limiting our confidence in the role of VOC entrainment into the evolving plume. Due to this uncertainty we are assuming the lower limit of VOC and NO_x over the lake, with O_3 and NO_x only changing as much as 2.3% and 3.2%, respectively as an upper limit.

Estimates of k_{dil} over land for urban plumes have been made using measurements of the dispersion of conserved tracers (Müller et al., 2015) and range between 0.23 h^{-1} for the Sacramento plume (Dillon et al., 2002), 0.20-0.22 h^{-1} for the Nashville plume (Nunnermacker et al., 1998) and 0.1 h^{-1} for the Toronto plume (X. Lin et al., 1996). Consistent with these determinations, we set k_{dil} over land at 0.2 h^{-1}. Over water and just onshore, there is little change in the mixed layer height from 10:00-17:00 CDT as obtained from HRRR, significantly reducing vertical dilution that can compose a considerable portion of k_{dil} (Dillon et al., 2002). Sillman et al. (1993) suggested that suppressed vertical mixing of the Chicago plume over Lake Michigan leads to high O_3 concentrations that match observations. To estimate entrainment rates over the lake, we use measurements of CO as conserved tracer. CO measurements from AQS monitors in East Chicago, IN and Milwaukee, WI were used to evaluate the dilution of a parcel passing through those two

points on 2 June and the lake specific dilution rate was estimated to be k_{dil} = 0.056 h^{-1} (τ_{mix} of 0.75 days; SI S6; Fig S15). This value is a best estimate, as such a tracer may be subject to local influences in Milwaukee. Figure 4c shows that the prescribed dilution rate has a significant effect on O_3 and NO_x concentrations, allowing for sustained and elevated O_3 over the lake where no emissions are provided. Unfortunately, routine measurements of conserved tracers are not available along the coastline, significantly limiting our observational constraints on $k_{dil.}$

To assess the spatial dependency of the model's initial and boundary conditions for plume simulations, the backward trajectory analysis from Zion, IL was repeated for the two hours preceding and following peak O_3 (15:00 – 19:00 CDT). Trajectories for the entire lake breeze period are shown in Fig. S17. Figure 5 shows the trajectory model results along with the associated trajectory paths that end at each designated hour in Zion. The model results are endpoint concentrations of a unique back trajectory that terminates at Zion at the marked time on Fig. 5. While the hourly measurements (colored lines) are not all in good agreement with the hourly model results (colored circles), most of the measurements when averaged over this period are in good agreement. Extending the averaging time to multiple hours, would confound the interpretation of the indicator ratio. During this 5-hour period, model averaged O_3, NO_x, and H_2O_2 are in reasonably good agreement with measurements: $[O_3]_{mod}$ = 79.2 ppbv, $[O_3]_{meas}$ = 85.1 ppbv, $[NO_x]_{mod}$ = 5.70 ppbv, $[NO_x^*]_{meas}$ = 6.12 ppbv, $[H_2O_2]_{mod}$ = 0.425 ppbv, $[H_2O_2]_{meas}$ = 0.458 ppbv. Model 5-hour average HNO_3 (which shown on a different scale in Fig. 5) during the lake breeze event (2.47 ppbv) is significantly larger than that measured (0.717 ppbv); potential reasons for this discrepancy are discussed below. Model and measured averages of each hourly H_2O_2/HNO_3 during this period are 0.267 and 0.625, respectively.

The temporal profile of modeled and measured HNO_3 agree well, where the mixing ratio of HNO_3 remains above 0.5 ppbv into the early evening. However, the modeled HNO_3 mixing ratio is as much as 4x larger than the observations. This discrepancy could be attributed to a number of processes: 1) The model has a fixed HNO_3 gas-particle partitioning rate constant (k_{uptake}) of 6 x10^{-5} s^{-1} although experimental observations of HNO_3 uptake coefficients allow k_{uptake} to aerosol particles to be between 10^{-5}-10^{-1}, quickly reaching equilibrium with the aerosol phase. There was no evidence of low-level clouds observed over Lake Michigan in the trajectory region on 2 June,

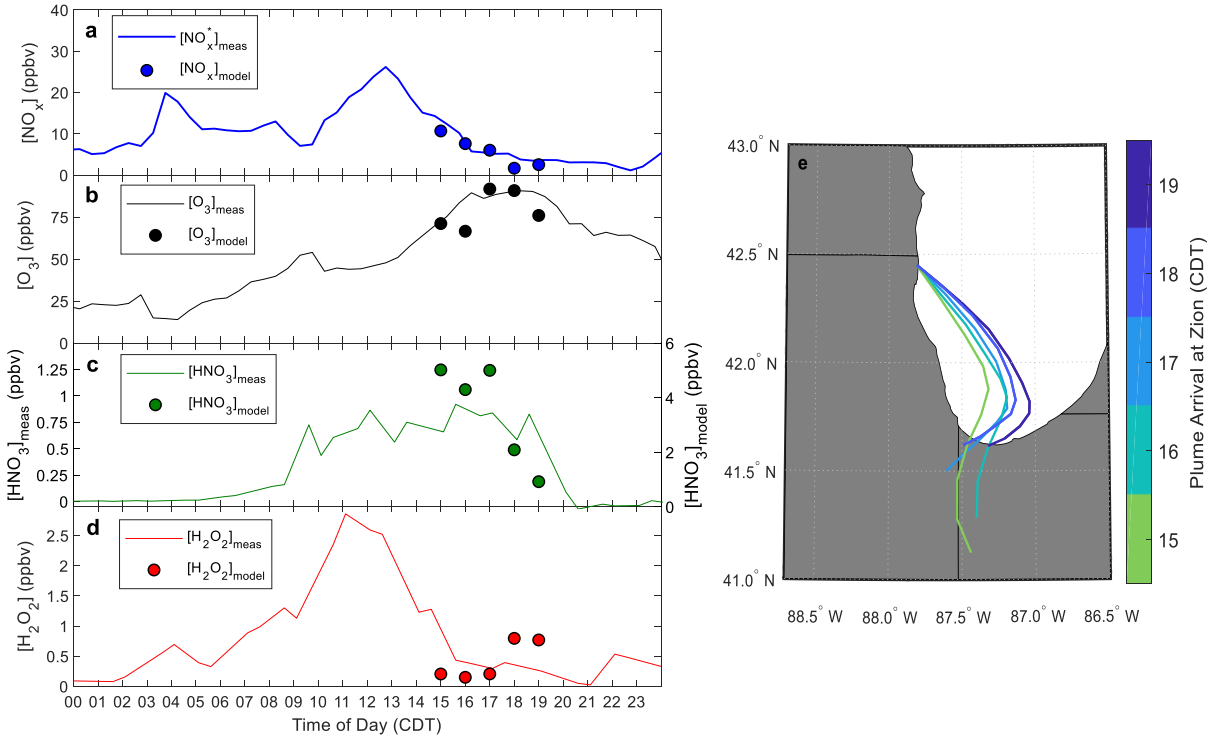

Figure 5: a-d) Comparison of modeled (colored dots) and half-hour average measurements (lines) of NO_x^*, O_3, HNO_3, and H_2O_2 mixing ratios at Zion, IL. To limit the analysis to trajectories spending most of the transit time over the lake, the modeled values considered are those at the base case (17:00 CDT) and two points on either side. Modeled and measured NO_x, O_3, and H_2O_2 mixing ratios are in good agreement, while modeled HNO_3 is overestimated by as much as a factor of 4. e) 10-hour HYSPLITT backward trajectories ending at Zion, IL corresponding to the designated plume arrival time.

suggesting that loss of HNO_3 to cloud was likely minimal although partitioning of HNO_3 to aerosol particles could account for a significant fraction of the model-measurement discrepancy. Springtime measurements of mixed rural and urban HNO_3 and NO_3^- show particulate NO_3^- to gaseous HNO_3 ratios ranging from 0.43:1 to 5.7:1 with an average of 2.9:1 (Danalatos & Glavas, 1999; Li et al., 2014; Y. Lin et al., 2006; Puxbaum et al., 1993; Song et al., 2011; Walker et al., 2004). This allows particulate NO_3^- to provide an upper and lower bound for a measured Sillman indicator by replacing $[HNO_3]$ with $([HNO_3]+[NO_3]^-)$, with $[NO_3^-]$ taken from onsite 12-hour collections of particulates. The impact of the particulate measurements at Zion on evaluation of the Sillman indicator determination for the 2 June case study are discussed in section 4.3. 2) HNO_3 deposition velocities, (v_d; cm s^{-1}) follow a diel cycle that can exceed 3 cm s^{-1} in forested regions (Nguyen et al., 2015) and can exceed 7 cm s^{-1} in urban areas (Nunnermacker et al., 1998; Pierson

et al., 1988). The model does not differentiate between forested and urban regions over land and uses a fixed parameterization (Johnson, 2010) for calculating v_d in low-moderate winds (<2 ms^{-1}) over the lake (v_d = 0.1 cm s^{-1}). Inaccuracies in land cover type, spatial variability of wind speed over the lake, and experimentally determined land v_d can contribute uncertainty in dry deposition rates. 3) Our trajectory model has only one vertical layer in the mixed layer, forcing all HNO_3 to be evaluated in a single layer. The measurements were made at 5m, significantly lower than the average height of the mixed layer. A strong vertical gradient in HNO_3, driven by surface deposition, would lead to a model-measurement disagreement. It has been shown that HNO_3 mixing ratios increase by about a factor of 1.3 with height due to a decrease in dry deposition further away from the surface, introducing a small source of uncertainty. (Huebert & Robert, 1985; Lee et al., 1993; Pryor et al., 2002).

In the following section, we utilize these measurements to discuss: 1) the sensitivity of H_2O_2 and HNO_3 to changes in NO_x and VOC emissions during the 2 June event, and 2) the utility of H_2O_2 and HNO_3 based indicators for providing unique constraints on the dependency of P_{O3} on VOC and NO_x.

4. Discussion

4.1 Sensitivity to NEI Emissions

The sensitivity of P_{O3} to NO_x and anthropogenic VOC was evaluated in the model by calculating the change in O_3 (ΔO_3) from the start of the trajectory to the arrival at Zion (2 June at 17:00 CDT) as a function of NO_x and anthropogenic VOC emission rates (Figure 6). NO_x and VOC emission rates shown in Figure 6 are normalized to the NEI base case (described in section 2.2) at E_{NOx} and E_{VOC} =1. In the base case, ΔO_3 = 53.3 ppbv or 5.33 ppbv hr^{-1} based on a 10 hr trajectory time. The grey dot on the isopleth in Fig. 6 indicates the base case model solution where E_{NOx} and E_{VOC} =1. Included on the isopleth is the ΔO_3 ridgeline (black solid line) which was calculated from the maxima of each contour. The measured ΔO_3 over this period was calculated by extrapolating out two hours from the Hammond, IL AQS site value in Figure 4a. This measured ΔO_3 is shown with the dashed contour (ΔO_3 = 51 ppbv). Above the ridgeline O_3 production is VOC-sensitive; where increasing E_{VOC} increases ΔO_3 and increasing E_{NOx} decreases ΔO_3. Below the ridgeline, O_3 production is NO_x-sensitive; where increasing E_{NOx} increases ΔO_3 and increasing E_{VOC} has a small

effect on ΔO_3. It is evident that in the base case simulation, the cumulative O_3 production integrated through the air mass transit to Zion is strongly VOC-sensitive. The O_3 isopleth developed for the 2 June trajectory reaching Zion at 17:00 CDT also highlights the strong sensitivity of O_3 production to subtle changes in anthropogenic NO_x and VOC emissions. For example, an increase in either E_{NOx} or E_{VOC} by 10% in any direction can change ΔO_3 by as much as 13%. VOC-sensitive O_3 production, as shown in Figure 6, is consistent with the high HNO_3/H_2O_2 ratios observed at the Zion field site during lake breeze (Fig. 3c).

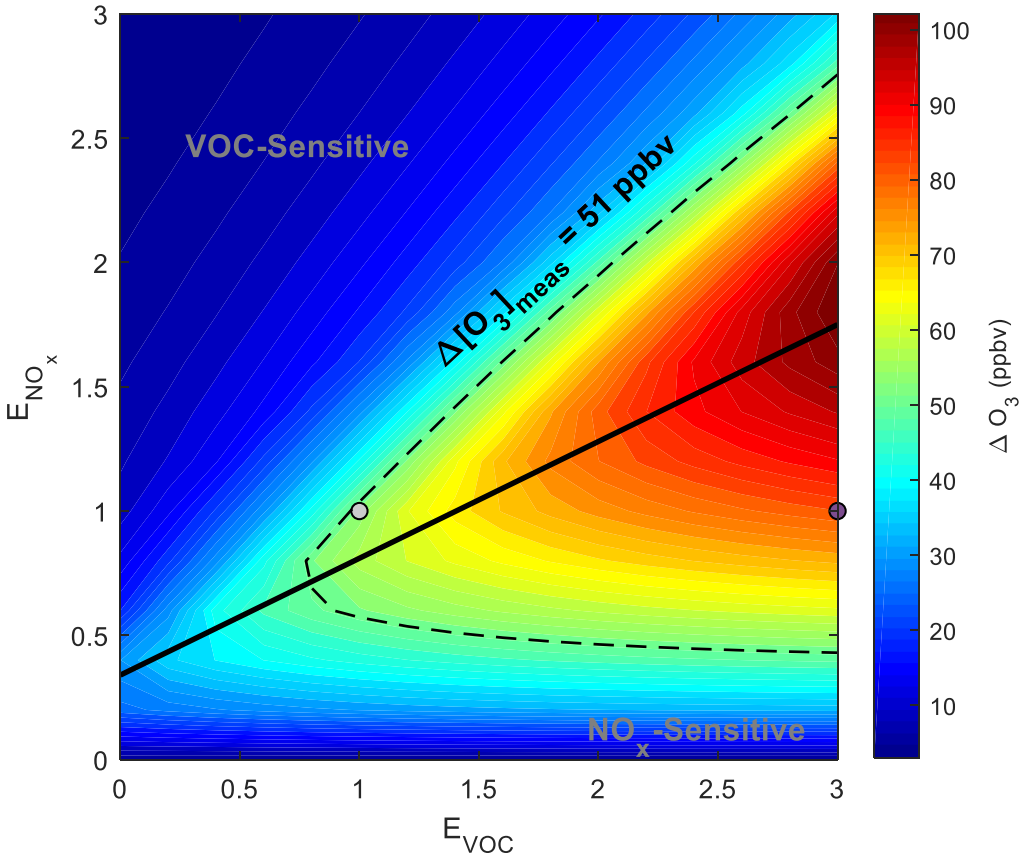

Figure 6: Calculated increase in O_3 between the start (8:00 CDT) and end of the model trajectory that arrives at Zion, IL at 17:00 CDT on 2 June 2017. Isopleths in ΔO_3 were generated by varying NO_x and anthropogenic VOC emissions, E_{NOx} and E_{VOC}, relative to the base case where E_{NOx} and E_{VOC} =1. Indicated by points are the E_{NOx} and E_{VOC} =1 (grey) E_{NOx}=1 and E_{VOC} =3 (purple) solutions. The model base case ΔO_3 suggests that O_3 formation is in a VOC-sensitive regime. The dashed contour corresponds to measured $\Delta[O_3]$ during this period and the solid line is the NO_x-VOC sensitivity transition line as calculated from the isopleth ridgeline.

512 The largest source of uncertainty in calculating O_3 production rates lies in the quantity and
513 speciation of VOC emissions. To assess the accuracy of NEI VOC emissions, the VOC reactivity
514 (VOCR; s^{-1}) to OH was calculated and compared to measured values at the Zion endpoint. The
515 total VOC reactivity is calculated as:

516 $$VOC_{R,total} = \sum k_{OH+X_i}[X_i] \quad (E4)$$

517 where k_{OH+Xi} is the rate constant for a reaction of OH with a specific VOC and $[X_i]$ is the ambient
518 concentration of the VOC. Rate constants used in this analysis were taken from the MCM v3.2
519 (Bloss et al., 2005; Jenkin et al., 2015; Jenkin et al., 1997; Saunders et al., 2003). Figure 7a shows
520 the time progression of modeled VOCR along the airmass trajectory leading to Zion for the base
521 case simulation and a simulation where all anthropogenic VOC emissions are increased by a factor
522 of 3 in order to determine model VOCR sensitivity to VOC emissions and to simulate a case of
523 NO_x sensitivity in the source region. Increasing VOC emissions by this much shifts ozone
524 production into the NO_x-sensitive regime, as shown in Figure 6. Carbon monoxide chemistry is
525 included in the model, but the contribution of CO to VOCR is not shown in Figure 7a as there was
526 no reliable CO measurement at Zion for comparison. In the model, CO contributes to 38% of the
527 total VOCR. Also included on Figure 7a is the experimentally determined VOCR at the end of the
528 simulation, determined using measured VOC concentrations taken from the *in situ* PTR-MS
529 observations, offline canister samples, and PAMS measurements. Measured HCHO was taken
530 from the PAMS regional average of 4.1 ppbv and it is estimated that the VOCR associated with
531 HCHO is close to the Zion area within a factor of two.

The base case modeled and measured VOCR are in excellent agreement, while the 3x emissions

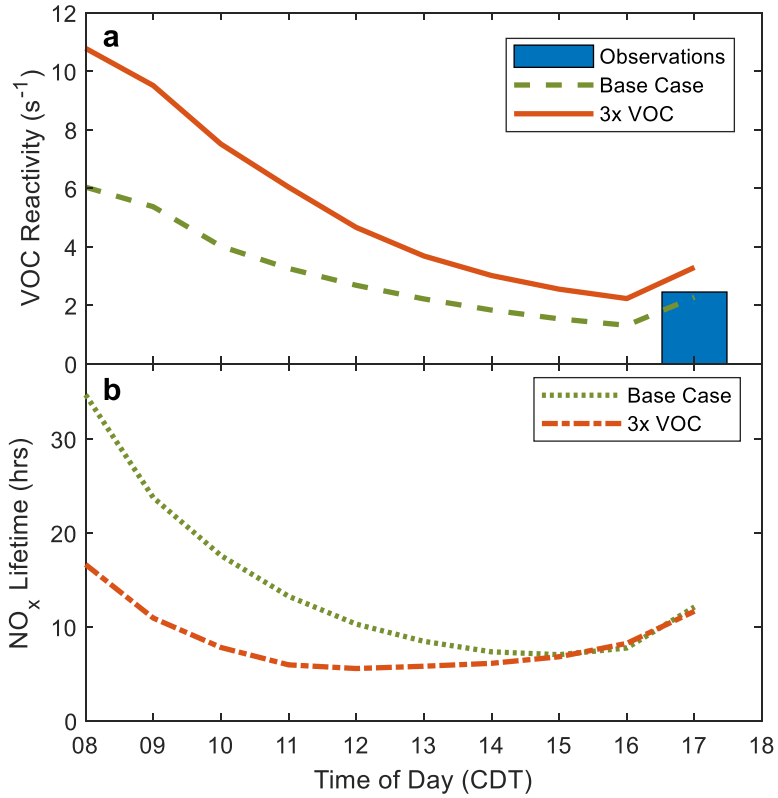

Figure 7: VOC reactivity (a) and NO_x lifetime (b) for the base case and 3x anthropogenic VOC case. The bar graph in panel A shows the measured VOCR according to PTR-MS, canister, and PAMS measurements. The major contributors of measured VOCR are HCHO (34.6%), isoprene (29.4%), acetaldehyde (11.2%), acetone (6.7%), methanol (4.5%), ethane/propane/butane (4.0%), xylenes (3.7%), MVK/MACR (3.4%), monoterpenes (1.3%), toluene (0.8%), ethene (0.3%), and benzene (.1%).

case overestimates the observed VOCR by 39%. At the start of the trajectory, the VOCR of 6.0 s^{-1} is comparable to estimates from NO_x-polluted urban sites that exclude consideration of CO contribution removed such as Phoenix (VOCR = 4.9 s^{-1}; NO_x = 21 ppbv), Philadelphia (VOCR = 6.8 s^{-1}; NO_x = 35 ppbv), (Kleinman et al., 2002) and Houston (VOCR= 8.7 s^{-1}; NO_x = 22 ppbv) (Mao et al., 2010). At the end of the trajectory, local BVOC emissions are entrained into the air mass, rapidly increasing VOCR leading to a significant contribution from local isoprene emissions. The entrainment of local BVOC, in a region and over a timescale where little O_3 is formed, complicates the direct interpretation of VOCR and P_{O3} and this site.

In parallel, it is expected that the NO_x lifetime ($\tau_{NOx,chemical}$; hrs) to OH will be impacted by both the prescribed NO_x and VOC emission rates. In the model, a total NO_x lifetime (τ_{NOx}; hrs) is solved, accounting for both the chemical loss and dilution.

$$\tau_{NO_x} = \frac{1}{k_{NO_x+OH}[OH] + k_{dil}([NO_x] - [NO_x]_b)} \quad (E5)$$

NO_x lifetimes are calculated from the observed loss of NO_x within the plume either *via* column retrieval from remote sensing products or from surface measurements in multiple ground stations (Liu et al., 2016; Nunnermacker et al., 2000). The reported NO_x lifetime in these scenarios is a function of both k_{dil} and k_{NOx+OH} as the lifetime depends on chemical loss to NO_z as well as 3D ventilation. Figure 7b shows τ_{NOx} in both the base and 3x anthropogenic VOC cases. In the base case simulation, the NO_x lifetime (τ_{NOx}) starts at 34.8 hours ($\tau_{NOx\text{-}mix,\ land}$ = 5 hrs, 8AM), and rapidly decreases to 10.7 hours by solar noon ($\tau_{NOx\text{-}mix,\ water}$ = 18 hrs), where $\tau_{NOx\text{-}mix}$ is the mixing lifetime of NO_x, or, k_{dil}^{-1}. In the 3x VOC simulation, the NO_x chemical lifetime is comparatively stable, starting at 16.5 hours and ending at 11.7 hours, showing a transition to VOC dominant OH reactions and high, sustained [OH]. The decrease in τ_{NOx} in the 3x VOC case is largely the result of increased [OH] from enhanced $P(HO_x)$ resulting from larger HCHO and carbonyl emissions. Plume profiles of [OH] and other important chemical species from the base case and 3x VOC simulations are provided in Figures S18-S19. As expected for a weakly ventilated plume passing over a lake, τ_{NOx} in each case is higher than many studies of continental summertime and springtime NO_x-polluted plumes (2-10 hours) (de Foy et al., 2015; Liu et al., 2016; Martin, 2003; Nunnermacker et al., 2000; Ryerson, 2003).

In the case of a weakly ventilated urban plume transported via lake breeze, chemical reactions determine both VOCR and the lifetime of NO_x. The model-measurement comparison of VOCR and τ_{NOx} also provides insight into the factors that control O_3 production. In the base case, VOCR decreases more slowly than τ_{NOx}, indicating faster NO_x termination, again indicative of a VOC-sensitive regime. In the 3x VOC case, VOC is lost to OH faster than NO_x, indicating NO_x-sensitive O_3 production. As shown in Fig. 4a, monitors of O_3 located near the parcel's lake entrance and at Zion as well as the Zion NO_x measurements suggest that the base case more accurately represents the chemistry of the evolving plume. Under the 3x anthropogenic VOC case the mixing ratios of

572 O_3 and NO_x at Zion are calculated to be 166 and 3.4 ppbv, significantly different than the
573 observations (Fig. S19).
574
575 *4.2 Indicators of Instantaneous O_3 Production*
576 As discussed in section 1, simultaneous measurements of the termination products of NO_x and
577 HO_x reactions should provide direct insight on O_3-NO_x-VOC-sensitivity in the urban-sourced Lake
578 Michigan plume. As illustrated in Figure 2, the sensitivity of O_3 production at the Zion site, as
579 defined by the ensemble average in H_2O_2/HNO_3 appears to indicate NO_x-sensitivity on average.
580 In contrast, the 2 June O_3 exceedance event presented in Section 4.1 indicates that O_3 production
581 in this airmass was largely VOC-sensitive. To shed light on these differences, we start by
582 evaluating indicators derived from instantaneous production rates: P_{H2O2}/P_{HNO3} (Fig. 8a), the
583 fraction of radicals lost to NO_x (L_N/Q) (Fig 8b), and net $P(O_3)$ (net $P(O_3) = P_{O3}$-L_{O3}) calculated
584 along the trajectory for the base case simulation. The P_{H2O2}/P_{HNO3} indicator is calculated using E1
585 which serves as a good estimation for P_{H2O2} and P_{HNO3} in urban, low-BVOC plumes. The L_N/Q
586 value was calculated using E2, also accounting for nitrous acid (HONO) production and loss in
587 the L_N and Q terms respectively, as HONO may be a large source of HO_x in the lower atmosphere
588 (Su et al., 2011). We evaluate the indicator ratios along the trajectory from 9:00 to 17:00 CDT,
589 with the parcel position at 9:00 being the last position the air mass travels over in the source region
590 before being advected over the lake. Net $P(O_3)$ increases from 2.1 to 10.2 ppbv hr^{-1} with peak
591 production occurring near 13:00 CDT. At 9:00 CDT, the relative rates of P_{HNO3} and P_{H2O2} is
592 indicative of a NO_x-saturated, VOC-sensitive plume, with P_{HNO3} exceeding P_{H2O2} by over three
593 orders of magnitude. Calculation of P_{HNO3} along the trajectory indicates that P_{HNO3} peaks around
594 noon and steadily declines throughout the rest of the trajectory as NO_x is consumed.
595 Commensurate with NO_x removal, chain termination resulting in H_2O_2 production steadily
596 increases. The profile of Q also indicates an increase in VOC oxidation and ultimately termination
597 to H_2O_2 as a predominant path as NO_x is consumed.
598
599 The P_{H2O2}/P_{HNO3} indicator, calculated along the trajectory, depicts the urban plume as moving from
600 a strongly VOC-sensitive regime ($P_{H2O2}/P_{HNO3} = 2.5 \times 10^{-4}$) towards the NO_x-sensitive transition
601 regime by the time it reaches Zion ($P_{H2O2}/P_{HNO3} = 0.03$). The fraction of radical loss to NO_x (L_N/Q)

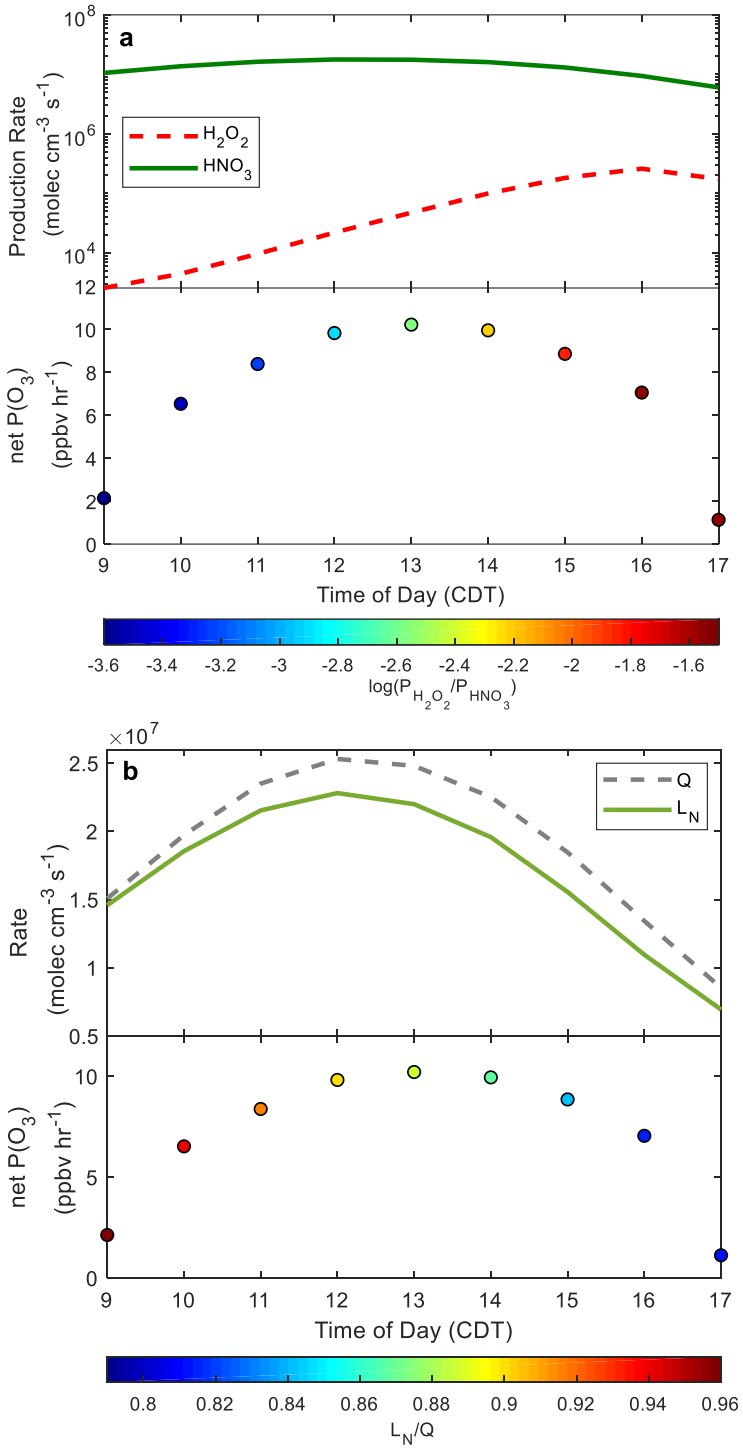

Figure 8: a) Modeled production rates of HNO_3 and H_2O_2 along the parcel trajectory from the Gary-Chicago area to Zion and net $P(O_3)$ colored by $\log(P_{H2O2}/P_{HNO3})$. P_{HNO3} peaks around noon and subsequently decreases while P_{H2O2} increases throughout the trajectory. b) L_N and Q along the trajectory and net $P(O_3)$ colored by L_N/Q. Both indicators show agreement with a transition from VOC-limited at the start of the trajectory to more NO_x-limited.

602

603 also indicates this transition. Radical removal changes from almost complete radical removal to
604 NO_x (L_N/Q = 0.95), indicating VOC-sensitivity, towards the literature transition region of NO_x-
605 sensitive fraction of radical loss (0.4-0.6) as the plume arrives at the Zion site (L_N/Q = 0.80). For
606 both instantaneous indicators, the peak of net $P(O_3)$ occurs in a highly VOC-sensitive regime,
607 which is difficult to conclude from the model or measured endpoint H_2O_2/HNO_3 at Zion. This
608 analysis suggests that in order to fully exploit the utility of the Sillman indicator to understand O_3
609 production in an evolving plume, more ground-based measurements along the plume trajectory are
610 required. The measurements on both ends of the plume should include the termination products,
611 HNO_3 and H_2O_2, as well as a measurement of particulate nitrate, NO_x, VOC, and CO as a passive
612 tracer for plume dilution.
613
614 *4.3 Integrated and Instantaneous P_{H2O2} and P_{HNO3} in the Context of Available Precursors*
615 Model calculations of H_2O_2/HNO_3, at the Zion endpoint on 2 June at 17:00 CDT, are shown in
616 Figure 9a as a function of the prescribed NO_x and anthropogenic VOC emission rates. The ΔO_3
617 ridgeline (from Fig. 6) is also shown to distinguish regions of VOC- and NO_x-sensitive chemistry.
618 Campaign average H_2O_2/HNO_3, as measured at Zion during lake breeze circulation during this
619 time period (dotted line; H_2O_2/HNO_3 = 3.3), and H_2O_2/HNO_3 measured on 2 June at 17:00 CDT
620 (dashed line; H_2O_2/HNO_3 = 0.49) are also shown as contours in Figure 9a. The ΔO_3 ridgeline
621 derived from the O_3 isopleth figure suggests a transition region for the Sillman indicator as it
622 crosses the log(H_2O_2/HNO_3) contours. The ridgeline encompasses model solutions for
623 H_2O_2/HNO_3 of 0.10-0.35, establishing a threshold between VOC and NO_x limited O_3 production.
624 The model solution for the base case (E_{NOx} and E_{VOC} =1) is determined to be H_2O_2/HNO_3 = 0.041
625 and is found outside of the transition region, firmly in the VOC-sensitive regime. As discussed
626 previously, campaign averaged H_2O_2/HNO_3 (3.3) suggests that O_3 production at Zion is in a very
627 NO_x-sensitive regime, while the observed ratio on 2 June at 17:00 CDT (during peak O_3 associated
628 with lake breeze circulation) suggests that O_3 production resides closer to the NO_x- to VOC-
629 sensitive transition and would be within the VOC sensitive regime if particulate nitrate was
630 included in the analysis.
631
632 This analysis highlights the challenges associated with using observationally constrained indicator

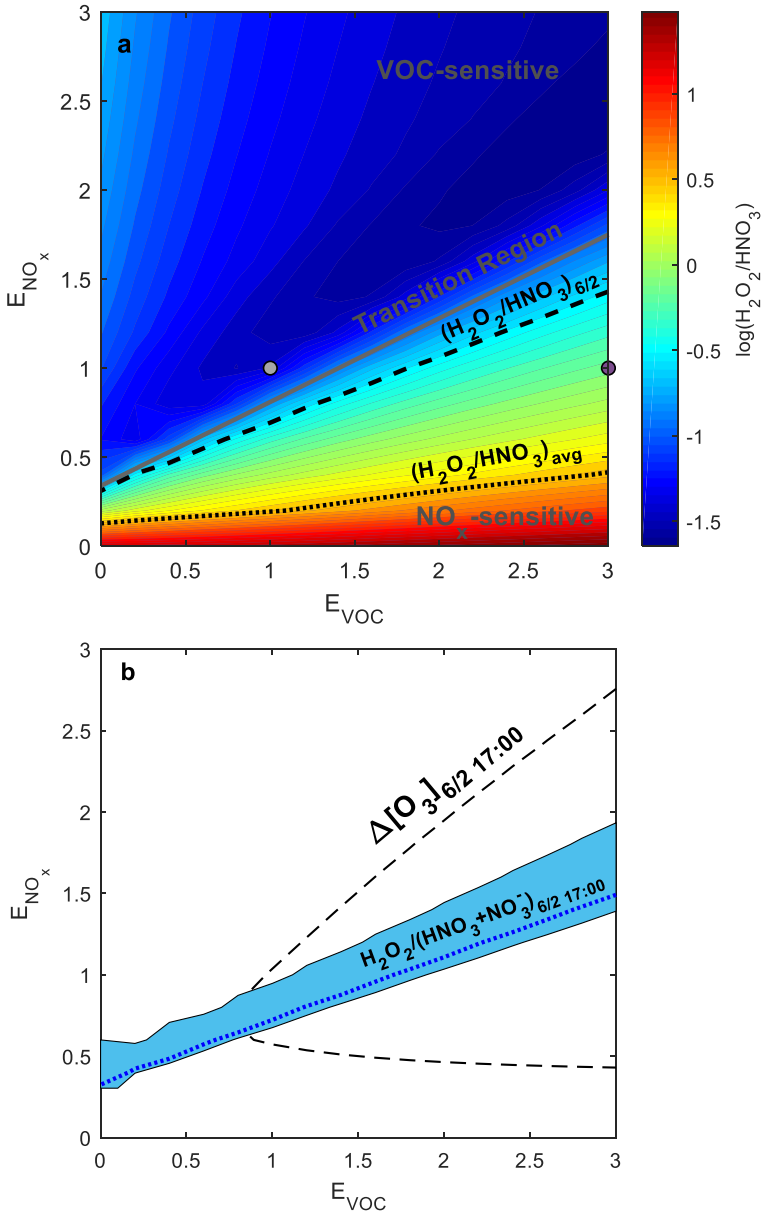

Figure 9: a) Model calculations of H_2O_2/HNO_3, at the Zion endpoint on 2 June at 17:00 CDT, as a function of the prescribed NO_x and anthropogenic VOC emission rates. The ΔO_3 ridgeline (from Fig. 8, solid grey line) is shown to distinguish regions of VOC- and NO_x-sensitive chemistry. Campaign average H_2O_2/HNO_3, as measured at Zion during lake breeze circulation (dotted line; H_2O_2/HNO_3 = 3.3), and H_2O_2/HNO_3 measured on 2 June at 17:00 CDT (dashed line; H_2O_2/HNO_3 = 0.35) are also shown as contours. Also shown are the base case (grey point) and 3x VOC (purple point) solutions. b) The model ΔO_3 contour line that is consistent with measured ΔO_3 for 2 June 17:00 CDT (grey dashed line) is shown alongside the model H_2O_2/HNO_3 contour lines that are consistent with measurements of H_2O_2, HNO_3, and estimates or measurements of particulate NO_3^- (estimates, blue shaded region; measured, blue dotted line). The bounds of the shaded region are set by NO_3^- = 0 ppbv and NO_3^- = 2.9 × [HNO_3].

633

ratios at measurement sites influenced by a wide number of source regions: 1) regional air masses of high BVOC and low NO_x display large H_2O_2/HNO_3 ratios and 2) urban plumes with elevated NO_x are characterized by much smaller H_2O_2/HNO_3 ratios. The mixing of these air masses dilutes the information content of the indicator and the utility of H_2O_2/HNO_3 for describing the chemical regime under which the observed O_3 was produced in. Analysis of the trajectory ending at Zion on 2 June at 17:00 CDT was chosen to minimize the challenges associated with the mixing of these two sources as the urban plume mixes over the lake on its trajectory to Zion. This analysis underscores the utility of high time resolution measurements of H_2O_2 and HNO_3 that can be used to study individual plumes associated with lake breeze circulation.

In theory, coincident measurements of ΔO_3 and H_2O_2/HNO_3 provide unique constraints on both the sensitivity regime where O_3 is produced and the prescribed NO_x and VOC emission rates used in chemical transport models. In Figure 9b the model ΔO_3 contour line that is consistent with measured ΔO_3 for 2 June 17:00 CDT is shown alongside the model H_2O_2/HNO_3 contour line that is consistent with measurements of H_2O_2, HNO_3, and estimates of particulate NO_3^-. Assuming that the trajectory model captures the correct chemistry and physics of the evolving urban plume, the overlap of the ΔO_3 contour with the $H_2O_2/(HNO_3+NO_3^-)$ contour represent unique solutions for E_{NOx} and E_{VOC}. The range in estimates of $H_2O_2/(HNO_3+NO_3^-)$ stem from the uncertainty in NO_3^-. The lower bound is set as $[NO_3^-] = 0$ ppbv and the upper bound is set as $[NO_3^-] = 2.9 \times [HNO_3]$, where 2.9 is an average of NO_3^-/HNO_3 taken from representative literature values. We also include a contour for $H_2O_2/(HNO_3+ NO_3^-)$ with a NO_3^-:HNO_3 of 0.36, which is the average NO_3^-/HNO_3 determined from the 12 hour daytime NO_3^- measurement and the concurrent averaged HNO_3 observations at Zion on June 2. This contour is nearly equivalent to the lower bound and assumes that particulate nitrate is not lost to dry deposition along the trajectory. From Figure 9b it is evident that this representation of the Sillman indicator places a bound on E_{NOx} and E_{VOC}. We suggest that future measurements include high time resolution measurements of particulate nitrate.

The constrained model of instantaneous P_{H2O2} and P_{HNO3} provides a more intuitive depiction of how NO_x and VOC in the source region as well as in the plume contribute to O_3 formation. Figure 10 depicts the time-dependent evolution of P_{H2O2}/P_{HNO3} tracked with VOCR and NO_x mixing ratio in ppbv. The indicator solutions shown in Figure 10 were generated from multiple model

simulations where the normalized NO_x and anthropogenic VOC emissions (E_{NOx} and E_{VOC}) are varied between 0 and 3. In this depiction the termination products of HO_x-NO_x chemistry are dictated by the concentration of NO_x. The first point, at 9:00 CDT, is found at a VOCR of 5.4 s^{-1} and NO_x mixing ratio of 24.8 ppbv. The trajectory follows a depletion of both NO_x and VOC resulting in a VOCR of 2.3 s^{-1} and a NO_x mixing ratio of 6.0 ppbv when the plume arrives at Zion. Mapping out the relative reactivities highlights the utility of an instantaneous indicator and its ability to characterize the O_3-HO_x-NO_x chemistry. In theory, the observation-based indicator, H_2O_2/HNO_3 would work in a similar way if the initial conditions of H_2O_2 and HNO_3 were the same and the loss rates of H_2O_2 and HNO_3 to dry deposition, reactive uptake to aerosol, and dilution were equal.

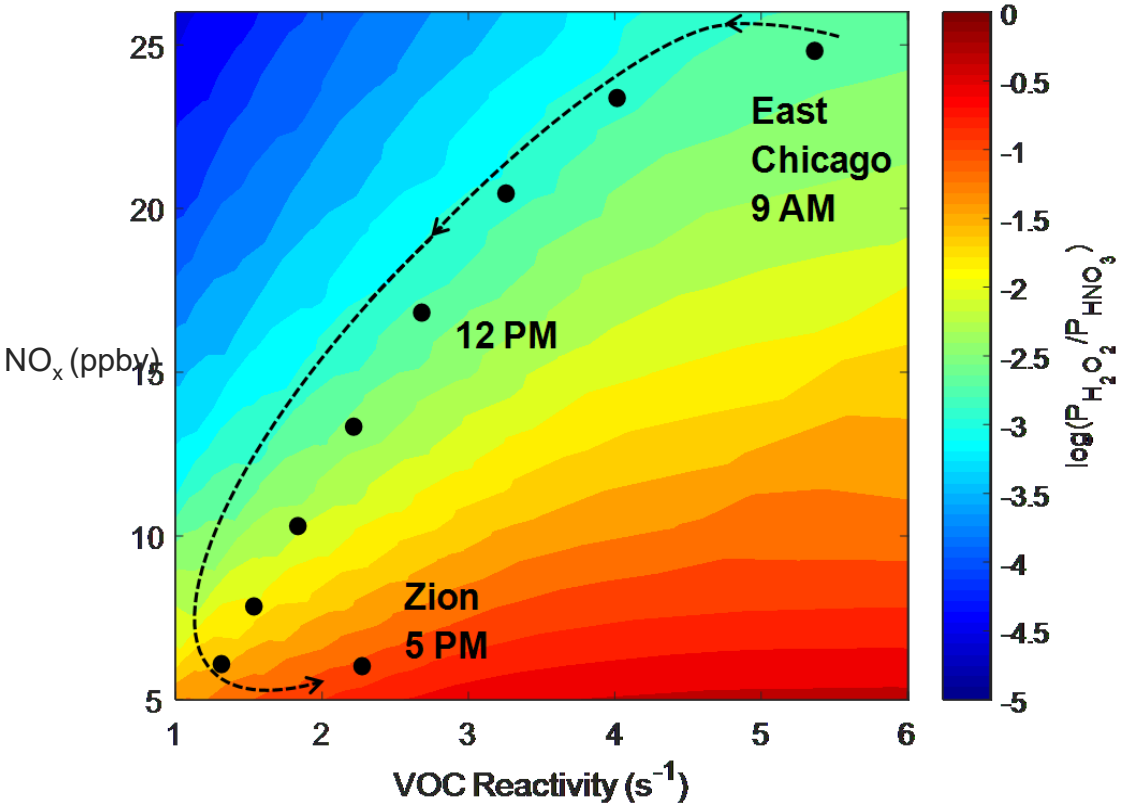

Figure 10: Model response of the instantaneous indicator P_{H2O2} / P_{HNO3} to VOCR and NO_x along the trajectory connecting the Chicago-Gary source region to Zion, IL. The representation starts at 9:00 CDT with VOCR (5.4 s^{-1}) and NO_x (24.8 ppbv) and ends at Zion at 17:00 CDT, where model VOCR = 2.3 s^{-1} and NO_x = 6.0 ppbv.

5. Conclusions

Elevated mixing ratios of O_3 in coastal regions are the product of intense photochemistry in concentrated urban plumes coupled with widespread lake or sea breeze circulation. This makes characterizing the O_3-NO_x-VOC sensitivity particularly challenging, especially when the urban plume evolves chemically along a trajectory between the source region and a receptor site with chemical measurements existing only at the end points. In this study, we investigated a specific high NO_x and O_3 event associated with lake-land breeze circulation along the coastline of Lake Michigan. A chemical trajectory model, constrained by a large suite of measurements from LMOS 2017, publicly available EPA ground-station data, the EPA NEI 2014, NASA remote sensing and model products, and NOAA meteorological data was developed to understand the NO_x-VOC sensitivity of coastal high O_3 events. Alongside model analyses, we explored the use of observational indicator ratios based on the concentrations of H_2O_2 and HNO_3 for describing the sensitivity of O_3 production to VOC and NO_x emissions.

Our results based on the 2 June 2017 high ozone event day indicate that the Chicago-Gary urban plume, as it advects north over Lake Michigan, transitions from an O_3 production regime that is VOC-sensitive towards a more NO_x-sensitive regime as it reaches receptor sites along Lake Michigan. Future studies should also examine the sensitivity of ozone formation to VOC and NOx on other high ozone days, particularly days with lower NO_x. Such work is crucial to determine whether the VOC sensitivity observed on 2 June 2017 is widely representative of ozone formation in this environment. We discuss the utility of the observation-based indicator H_2O_2/HNO_3, and the challenges associated with using time averaged measurements in complex sampling regions characterized by very different H_2O_2/HNO_3 ratios. We show that the assessments of NO_x-VOC sensitivity based on aggregate measurements of H_2O_2 and HNO_3 are not representative of urban plume chemistry, while measurements of H_2O_2/HNO_3 in individual lake breeze events accurately describe the sensitivity of O_3 production to VOC and NO_x as the integral of chemical production along the plume path. To fully leverage chemical indicators based on H_2O_2 and HNO_3 in this region, future measurements should include observations of H_2O_2, HNO_3, NO_x, VOC, and HO_x at the source region as well as at a lake breeze receptor region.

Acknowledgements and Data

The authors thank everyone involved with the Zion Supersite and LMOS 2017. We also thank Glenn Wolfe for developing his F0AM model and making it publicly available on his Github repository. This work was funded by the National Science Foundation under Grants No. AGS-1713001, AGS-1712828, and AGS-1712909. Any opinions, findings, and conclusions or recommendations expressed in this material are those of the authors and do not necessarily reflect the views of the National Science Foundation. The authors declare no competing interests. All field data from LMOS 2017 including the chemical and meteorological measurements presented in this manuscript is available on the NASA LaRC data archive at https://www-air.larc.nasa.gov/cgi-bin/ArcView/lmos. F0AM model outputs are available upon request.

References

Bertram, T. H., Kimmel, J. R., Crisp, T. a., Ryder, O. S., Yatavelli, R. L. N., Thornton, J. a., et al. (2011). A field-deployable, chemical ionization time-of-flight mass spectrometer. *Atmospheric Measurement Techniques*, *4*(7), 1471–1479. https://doi.org/10.5194/amt-4-1471-2011

Bloss, C., Wagner, V., Jenkin, M. E., Volkamer, R., Bloss, W. J., Lee, J. D., et al. (2005). Development of a detailed chemical mechanism (MCMv3.1) for the atmospheric oxidation of aromatic hydrocarbons. *Atmospheric Chemistry and Physics*, *3*(2002), 641–664.

Brook, J. R., Makar, P. A., Sills, D. M. L., Hayden, K. L., & McLaren, R. (2013). Exploring the nature of air quality over southwestern Ontario: Main findings from the Border Air Quality and Meteorology Study. *Atmospheric Chemistry and Physics*, *13*(20), 10461–10482. https://doi.org/10.5194/acp-13-10461-2013

Danalatos, D., & Glavas, S. (1999). Gas phase nitric acid, ammonia and related particulate matter at a Mediterranean coastal site, Patras, Greece. *Atmospheric Environment*, *33*, 3417–3425.

Devlin, R. B., McDonnell, W. F., Mann, R., Becker, S., House, D. E., Schreinemachers, D., & Koren, H. S. (1991). Exposure of humans to ambient levels of ozone for 6.6 hours causes cellular and biochemical changes in the lung. *American Journal of Respiratory Cell and Molecular Biology*, *4*(1), 72–81. https://doi.org/10.1165/ajrcmb/4.1.72

Dillon, M. B., Lamanna, M. S., Schade, G. W., & Goldstein, A. H. (2002). Chemical evolution of the Sacramento urban plume: Transport and oxidation. *Journal of Geophysical Research*, *107*(D5). https://doi.org/10.1029/2001JD000969

Dye, T. S., Roberts, P. T., & Korc, M. E. (1995). Observations of Transport Processes for Ozone and Ozone Precursors during the 1991 Lake Michigan Ozone Study. *American Meteorological Society*, *34*, 1877–1889.

Fehsenfeld, F. C., Dickerson, R. R., Hubler, G., Luke, W. T., Nunnermacker, L. J., Williams, E. J., et al. (1987). A ground-based intercomparison of NO, NO(x), and NO(y) measurement techniques. *Journal of Geophysical Research*, *92*(D12), 14710–14722. https://doi.org/10.1029/JD092iD12p14710

744 Foley, T., Betterton, E. A., Robert Jacko, P. E., & Hillery, J. (2011). Lake Michigan air quality: The
745 1994-2003 LADCO Aircraft Project (LAP). *Atmospheric Environment*, *45*(18), 3192–3202.
746 https://doi.org/10.1016/j.atmosenv.2011.02.033

747 de Foy, B., Lu, Z., Streets, D. G., Lamsal, L. N., & Duncan, B. N. (2015). Estimates of power plant NO x
748 emissions and lifetimes from OMI NO2 satellite retrievals. *Atmospheric Environment*, *116*(2015),
749 1–11. https://doi.org/10.1016/j.atmosenv.2015.05.056

750 Gauderman, W. J. (2006). Air Pollution and Children — An Unhealthy Mix. *New England Journal of*
751 *Medicine*, *355*(1), 78–79. https://doi.org/10.1056/NEJMe068096

752 Guenther, A., Karl, T., Harley, P., Wiedinmyer, C., Palmer, P. I., Geron, C., et al. (2006). Estimates of
753 global terrestrial isoprene emissions using MEGAN (Model of Emissions of Gases and Aerosols
754 from Nature). *Atmospheric Chemistry and Physics*, *6*, 3181–3210.

755 Harrison, P. R., & Winchester, J. W. (1971). Area-wide distribution of lead, copper, and cadmium in air
756 particulates from Chicago and northwest Indiana. *Atmospheric Environment (1967)*, *5*(10), 863–880.
757 https://doi.org/10.1016/0004-6981(71)90016-3

758 Huebert, B. J., & Robert, C. H. (1985). The Dry Deposition of Nitric Acid to Grass. *Journal of*
759 *Geophysical Research*, *90*(D1), 2085–2090.

760 Jacob, D. J. (1999). *Introduction to Atmospheric Chemistry*. Princeton, New Jersey: Princeton University
761 Press.

762 Jayarathne, T., Stockwell, C. E., Yokelson, R. J., Nakao, S., & Stone, E. A. (2014). Emissions of Fine
763 Particle Fluoride from Biomass Burning. *Environmental Science & Technology*, *48*, 12636–12644.
764 https://doi.org/10.1021/es502933j

765 Jenkin, M. E., Saunders, S. M., & Pilling, M. J. (1997). The tropospheric degradation of volatile organic
766 compounds: A protocol for mechanism development. *Atmospheric Environment*, *31*(1), 81–104.
767 https://doi.org/10.1016/S1352-2310(96)00105-7

768 Jenkin, M. E., Young, J. C., & Rickard, A. R. (2015). The MCM v3.3.1 degradation scheme for isoprene.
769 *Atmospheric Chemistry and Physics*, *15*(20), 11433–11459. https://doi.org/10.5194/acp-15-11433-
770 2015

771 Jerret, M., Burnett, R. T., Pope III, A., Ito, K., Thurston, G., Krewski, D., et al. (2009). Long-Term Ozone
772 Exposure and Mortality, 1085–1095.

773 Johnson, M. T. (2010). A numerical scheme to calculate temperature and salinity dependent air-water
774 transfer velocities for any gas. *Ocean Science*, *6*(4), 913–932. https://doi.org/10.5194/os-6-913-2010

775 Kleinman, L. I. (2005). The dependence of tropospheric ozone production rate on ozone precursors.
776 *Atmospheric Environment*, *39*(3), 575–586. https://doi.org/10.1016/j.atmosenv.2004.08.047

777 Kleinman, L. I., Daum, P. H., Imre, D. G., Lee, J. H., Lee, Y. N., Nunnermacker, L. J., et al. (2000).
778 Ozone production in the New York City urban plume. *Journal of Geophysical Research*
779 *Atmospheres*, *105*(D11), 14495–14511. https://doi.org/10.1029/2000JD900011

780 Kleinman, L. I., Daum, P. H., Lee, Y.-N., Nunnermacker, L. J., Springston, S. R., Weinstein-Lloyd, J., &
781 Rudolph, J. (2001). Sensitivity of ozone production rate to ozone precursors. *Geophysical Research*
782 *Letters*, *28*(15), 2903–2906. https://doi.org/10.1523/JNEUROSCI.4349-08.2008.Serotonergic

783 Kleinman, L. I., Daum, P. H., Imre, D., Lee, Y.-N., Nunnermacker, L. J., Springston, S. R., et al. (2002).
784 Ozone production rate and hydrocarbon reactivity in 5 urban areas: A cause of high ozone
785 concentration in Houston. *Geophysical Research Letters*, *29*(10), 105-1-105–4.
786 https://doi.org/10.1038/s41467-018-04034-w

787 Lee, G., Zhuang, L., Huebert, B. J., & Meyers, T. P. (1993). Concentration Gradients and Dry Deposition
788 of Nitric Acid Vapor at the Mauna Loa Observatory , Hawaii. *Journal of Geophysical Research*,
789 *98*(D7), 12,661-12,671.

790 Li, Y., Schwandner, F. M., Sewell, H. J., Zivkovich, A., Tigges, M., Raja, S., et al. (2014). Observations
791 of ammonia, nitric acid, and fine particles in a rural gas production region. *Atmospheric*
792 *Environment*, *83*(3), 80–89. https://doi.org/10.1016/j.atmosenv.2013.10.007

793 Lin, X., Roussel, P. B., Laszlo, S., Taylor, R., Melo, O. T., Shepson, P. B., et al. (1996). Impact of
794 Toronto urban emissions on ozone levels downwind. *Atmospheric Environment*, *30*(12), 2177–2193.
795 https://doi.org/10.1016/1352-2310(95)00130-1

796 Lin, Y., Cheng, M., Ting, W., & Yeh, C. (2006). Characteristics of gaseous HNO2 , HNO3 , NH3 and
797 particulate ammonium nitrate in an urban city of Central Taiwan. *Atmospheric Environment*, *40*,
798 4725–4733. https://doi.org/10.1016/j.atmosenv.2006.04.037

799 Liu, F., Beirle, S., Zhang, Q., Dörner, S., He, K., & Wagner, T. (2016). NOx lifetimes and emissions of
800 cities and power plants in polluted background estimated by satellite observations. *Atmospheric*
801 *Chemistry and Physics*, *16*(8), 5283–5298. https://doi.org/10.5194/acp-16-5283-2016

802 Loughner, C. P., Tzortziou, M., Follette-Cook, M., Pickering, K. E., Goldberg, D., Satam, C., et al.
803 (2014). Impact of bay-breeze circulations on surface air quality and boundary layer export. *Journal*
804 *of Applied Meteorology and Climatology*, *53*(7), 1697–1713. https://doi.org/10.1175/JAMC-D-13-
805 0323.1

806 Lurmann, F. W., Lloyd, A. C., & Atkinson, R. (1986). A chemical mechanism for use in long-range
807 transport/acid deposition computer modeling. *Journal of Geophysical Research*, *91*(D10), 10905.
808 https://doi.org/10.1029/JD091iD10p10905

809 Mao, J., Ren, X., Chen, S., Brune, W. H., Chen, Z., Martinez, M., et al. (2010). Atmospheric oxidation
810 capacity in the summer of Houston 2006 : Comparison with summer measurements in other
811 metropolitan studies. *Atmospheric Environment*, *44*, 4107–4115.
812 https://doi.org/10.1016/j.atmosenv.2009.01.013

813 Martin, R. V. (2003). Global inventory of nitrogen oxide emissions constrained by space-based
814 observations of NO_2 columns. *Journal of Geophysical Research*, *108*(D17), 4537.
815 https://doi.org/10.1029/2003JD003453

816 Mazzuca, G. M., Ren, X., Loughner, C. P., Estes, M., Crawford, J. H., Pickering, K. E., et al. (2016).
817 Ozone production and its sensitivity to NO*x* and VOCs: Results from the DISCOVER-AQ field
818 experiment, Houston 2013. *Atmospheric Chemistry and Physics*, *16*(22), 14463–14474.
819 https://doi.org/10.5194/acp-16-14463-2016

820 Milford, J. B., Russell, A. G., & McRae, G. J. (1989). A New approach to photochemical pollution
821 control: Implications of spatial patterns in pollutant responses to reductions in nitrogen oxides and
822 reactive organic gas emissions. *Environmental Science and Technology*, *23*(10), 1290–1301.
823 https://doi.org/10.1021/es00068a017

824 Millet, D. B., Alwe, H. D., Chen, X., Deventer, M. J., Gri, T. J., Holzinger, R., et al. (2018). Bidirectional
825 Ecosystem − Atmosphere Fluxes of Volatile Organic Compounds Across the Mass Spectrum : How
826 Many Matter? *ACS Earth and Space Chemistry*, *2*, 764–777.
827 https://doi.org/10.1021/acsearthspacechem.8b00061

828 Mills, G., Hayes, F., Wilkinson, S., & Davies, W. J. (2009). Chronic exposure to increasing background
829 ozone impairs stomatal functioning in grassland species. *Global Change Biology*, *15*(6), 1522–1533.
830 https://doi.org/10.1111/j.1365-2486.2008.01798.x

831 Müller, M., Anderson, B., Beyersdorf, A., Crawford, J. H., Diskin, G., Eichler, P., et al. (2015). In situ
832 measurements and modeling of reactive trace gases in a small biomass burning plume. *Atmospheric*
833 *Chemistry and Physics Discussions*, *15*(21), 31501–31536. https://doi.org/10.5194/acpd-15-31501-
834 2015

835 Nguyen, T. B., Crounse, J. D., Teng, A. P., St Clair, J. M., Paulot, F., Wolfe, G. M., & Wennberg, P. O.
836 (2015). Rapid deposition of oxidized biogenic compounds to a temperate forest. *Proceedings of the*
837 *National Academy of Sciences of the United States of America*, *112*(5), E392-401.
838 https://doi.org/10.1073/pnas.1418702112

839 Nunnermacker, L. J., Imre, D., Daum, P. H., Kleinman, L., Lee, Y. N., Lee, J. H., et al. (1998).
840 Characterization of the Nashville urban plume on July 3 and July 18 , 1995. *Journal of Geophysical*
841 *Research*, *103*(D21), 28,129-28,148.

842 Nunnermacker, L. J., Kleinman, L. I., Imre, D., Daum, P. H., Lee, Y. N., Lee, J. H., et al. (2000). NOy
843 lifetimes and O3 production efficiencies in urban and power plant plumes: Analysis of field data.
844 *Journal of Geophysical Research Atmospheres*, *105*(D7), 9165–9176.
845 https://doi.org/10.1029/1999JD900753

846 Peng, Y. P., Chen, K. S., Lai, C. H., Lu, P. J., & Kao, J. H. (2006). Concentrations of H2O2and
847 HNO3and O3-VOC-NOxsensitivity in ambient air in southern Taiwan. *Atmospheric Environment*,
848 *40*(35), 6741–6751. https://doi.org/10.1016/j.atmosenv.2006.05.079

849 Peng, Y. P., Chen, K. S., Wang, H. K., & Lai, C. H. (2011). In situ measurements of hydrogen peroxide,
850 nitric acid and reactive nitrogen to assess the ozone sensitivity in Pingtung county, Taiwan. *Aerosol*
851 *and Air Quality Research*, *11*(1), 59–69. https://doi.org/10.4209/aaqr.2010.10.0091

852 Pierce, B., Kaleel, R., Dickens, A., Bertram, T., & Kenski, D. (2017). White Paper: Lake Michigan Ozone
853 Study 2017 (LMOS 2017), *2017*, 1–22.

854 Pierson, W. R., Brachaczek, W. W., Japar, S. M., Cass, G. R., & Solomon, P. A. (1988). Dry deposition
855 and dew chemistry in Claremont, California, during the 1985 nitrogen species methods comparison
856 study. *Atmospheric Environment (1967)*, *22*(8), 1657–1663. https://doi.org/10.1016/0004-
857 6981(88)90393-9

858 Pryor, S. C., Barthelmie, R. J., Jensen, B., Jensen, N. O., & Soresnen, L. L. (2002). HNO3 fluxes to a
859 deciduous forest derived using gradient and REA methods. *Atmospheric Environment*, *36*(August
860 2001), 5993–5999.

861 Puxbaum, H., Haumer, G., Moser, K., & Ellinger, R. (1993). Seasonal Variation of HNO3, HCl, SO2,
862 NH3 and Particulate Matter at a Rural Site in Northeastern Austria (Wolkersdorf, 240 m a.s.l.).
863 *Atmospheric Environment*, *27*(15), 2445–2447.

864 Rolph, G., Stein, A., & Stunder, B. (2017). Environmental Modelling & Software Real-time

865 Environmental Applications and Display sYstem : READY. *Environmental Modelling and*
866 *Software*, *95*, 210–228. https://doi.org/10.1016/j.envsoft.2017.06.025

867 Ryerson, T. B. (2003). Effect of petrochemical industrial emissions of reactive alkenes and NOx on
868 tropospheric ozone formation in Houston, Texas. *Journal of Geophysical Research*, *108*(D8), 4249.
869 https://doi.org/10.1029/2002JD003070

870 Saunders, S. M., Jenkin, M. E., Derwent, R. G., & Pilling, M. J. (2003). Protocol for the development of
871 the Master Chemical Mechanism, MCM v3 (Part A): Tropospheric degradation of non-aromatic
872 volatile organic compounds. *Atmospheric Chemistry and Physics*, *3*(1), 161–180.
873 https://doi.org/10.5194/acp-3-161-2003

874 Schauffler, S. M., Atlas, E. L., Blake, D. R., Flocke, F., Lueb, R. A., Lee-Taylor, J. M., et al. (1999).
875 Distributions of brominated organic compounds in the troposphere and lower stratosphere. *Journal*
876 *of Geophysical Research*, *104*, 21,513-21,535.

877 Sillman, S. (1995). The Use of NOy, H2O2, and HNO3 as indicators for ozone-NOx-hydrocarbon
878 sensitivity in urban locations. *Journal of Geophysical Research*, *100*(188), 14,175-14,188.

879 Sillman, S. (2002). Some theoretical results concerning O3-NOx -VOC chemistry and NOx -VOC
880 indicators. *Journal of Geophysical Research*, *107*(D22), 4659.
881 https://doi.org/10.1029/2001JD001123

882 Sillman, S., & West, J. J. (2009). Reactive nitrogen in Mexico City and its relation to ozone-precursor
883 sensitivity: Results from photochemical models. *Atmospheric Chemistry and Physics*, *9*(11), 3477–
884 3489. https://doi.org/10.5194/acp-9-3477-2009

885 Sillman, S., Logan, J. A., & Wofsy, S. C. (1990). The sensitivity of ozone to nitrogen oxides and
886 hydrocarbons in regional ozone episodes. *Journal of Geophysical Research*, *95*(D2), 1837–1851.
887 https://doi.org/10.1029/JD095iD02p01837

888 Sillman, S., Samson, P. J., & Masters, J. M. (1993). Ozone Production in Urban Plumes Transported Over
889 Water : Photochemical. *Journal of Geophysical Research*, *98*(D7), 12687–12699.

890 Sillman, S., He, D., Cardelino, C., & Imhoff, R. E. (1997). The Use of Photochemical Indicators to
891 Evaluate Ozone-NOx-Hydrocarbon Sensitivity: Case Studies from Atlanta, New York, and Los
892 Angeles. *Journal of the Air and Waste Management Association*, *47*(1), 1030–1040.
893 https://doi.org/10.1080/10473289.1997.10464407

894 Smith, T. L., Benjamin, S. G., Brown, J. M., Weygandt, S., Smimova, T., & Schwartz, B. (2008).
895 Convection forecasts from the hourly updated, 3-km High Resolution Rapid Refresh (HRRR)
896 Model. In *24th Conference on Severe Local Storms*. Savannah, GA: American Meteorolo.
897 https://doi.org/10.5216/ree.v6i3.836

898 Song, F., Shin, J. Y., Atresino, R. J.-A., & Gao, Y. (2011). Relationships among springtime ground-level
899 NOx, O3 and NO3 in the vicinity of highways in the US East Cost. *Atmospheric Pollution Research*,
900 *2*(3), 374–383. https://doi.org/10.5094/APR.2011.042

901 Stauffer, R. M., & Thompson, A. M. (2012). Bay breeze climatology at two sites along the Chesapeake
902 bay from 1986 – 2010 : Implications for surface ozone. *J. Atmos. Chem.*, *72*, 355–372.
903 https://doi.org/10.1007/s10874-013-9260-y

904 Stein, A. F., Draxler, R. R., Rolph, G. D., Stunder, B. J. B., Cohen, M. D., & Ngan, F. (2015). Noaa's

hysplit atmospheric transport and dispersion modeling system. *Bulletin of the American Meteorological Society*, *96*(12), 2059–2077. https://doi.org/10.1175/BAMS-D-14-00110.1

Stone, E. A., Snyder, D. C., Sheesley, R. J., Sullivan, A. P., Weber, R. J., & Schauer, J. J. (2008). Source apportionment of fine organic aerosol in Mexico City during the MILAGRO experiment 2006. *Atmospheric Chemistry and Physics*, *8*(5), 1249–1259. https://doi.org/10.5194/acp-8-1249-2008

Su, H., Cheng, Y., Oswald, R., Behrendt, T., Trebs, I., Meixner, F. X., et al. (2011). Soil Nitrite as a Source of Atmospheric HONO and OH Radicals. *Science*, *333*(September), 1616–1619.

Sullivan, J. T., Berkoff, T., Gronoff, G., Knepp, T., Pippin, M., Allen, D., et al. (2019). The Ozone Water-Land Environmental Transition Study: An Innovative Strategy for Understanding Chesapeake Bay Pollution Events. *Bulletin of the American Meteorological Society*, (February), 291–306. https://doi.org/10.1175/BAMS-D-18-0025.1

Tonnesen, G. S., & Dennis, R. L. (2000). Analysis of radical propagation efficiency to assess ozone sensitivity to hydrocarbons and NOx 2. Long-lived species as indicators of ozone concentration sensitivity. *Journal of Geophysical Research*, *105*(D7), 9213. https://doi.org/10.1029/1999JD900371

Travis, K. R., Jacob, D. J., Fisher, J. A., Kim, P. S., Marais, E. A., Zhu, L., et al. (2016). Why do models overestimate surface ozone in the Southeast United States ? *Atmos. Chem. Phys.*, *16*, 13561–13577. https://doi.org/10.5194/acp-16-13561-2016

US EPA. National Ambient Air Quality Standards for Ozone, 80 Federal Register § (2015).

Walker, J. T., Whitall, D. R., Robarge, W., & Paerl, H. W. (2004). Ambient ammonia and ammonium aerosol across a region of variable ammonia emission density, *38*, 1235–1246. https://doi.org/10.1016/j.atmosenv.2003.11.027

Williams, E. J., Baumann, K., Roberts, J. M., Bertman, S. B., Norton, R. B., Fehsenfeld, F. C., et al. (1998). Intercomparison of ground-based NOy measurement techniques. *Journal of Geophysical Research*, *103*(D17).

Winchester, J. W., & Nifong, G. D. (1971). Water Pollution in Lake Michigan by Trace Elements from Pollution Aerosol Fallout. *Water, Air, and Soil Pollution*, *1*(1), 50–64. https://doi.org/https://doi.org/10.1007/BF00280779

Wolfe, G. M., Marvin, M. R., Roberts, S. J., Travis, K. R., & Liao, J. (2016). The framework for 0-D atmospheric modeling (F0AM) v3.1. *Geoscientific Model Development*, *9*(9), 3309–3319. https://doi.org/10.5194/gmd-9-3309-2016

Xu, Z., Wang, T., Xue, L. K., Louie, P. K. K., Luk, C. W. Y., Gao, J., et al. (2013). Evaluating the uncertainties of thermal catalytic conversion in measuring atmospheric nitrogen dioxide at four differently polluted sites in China. *Atmospheric Environment*, *76*, 221–226. https://doi.org/10.1016/j.atmosenv.2012.09.043